# Structural, Spectroscopic, and Theoretical Comparison of Traditional vs Recently Discovered Ln²⁺ Ions in the [K(2.2.2-cryptand)][(C₅H₄SiMe₃)₃Ln] Complexes: The Variable Nature of Dy²⁺ and Nd²⁺

Megan E. Fieser, Matthew R. MacDonald, Brandon T. Krull, Jefferson E. Bates, Joseph W. Ziller, Filipp Furche,* and William J. Evans*

Department of Chemistry, University of California, Irvine, California 92697-2025, United States

Ⓢ *Supporting Information*

ABSTRACT: The Ln^{3+} and Ln^{2+} complexes, Cp'_3Ln, **1**, (Cp' = $C_5H_4SiMe_3$) and [K(2.2.2-cryptand)][Cp'_3Ln], **2**, respectively, have been synthesized for the six lanthanides traditionally known in +2 oxidation states, i.e., Ln = Eu, Yb, Sm, Tm, Dy, and Nd, to allow direct structural and spectroscopic comparison with the recently discovered Ln^{2+} ions of Ln = Pr, Gd, Tb, Ho, Y, Er, and Lu in **2**. **2-La** and **2-Ce** were also prepared to allow the first comparison of all the lanthanides in the same coordination environment in both +2 and +3 oxidation states. **2-La** and **2-Ce** show the same unusual structural feature of the recently discovered +2 complexes, that the Ln–(Cp′ ring centroid) distances are only about 0.03 Å longer than in the +3 analogs, **1**. The Eu, Yb, Sm, Tm, Dy, and Nd complexes were expected to show much larger

differences, but this was observed for *only four of these traditional six* lanthanides. **2-Dy** and **2-Nd** are like the new nine ions in this tris(cyclopentadienyl) coordination geometry. A DFT-based model explains the results and shows that a $4f^n5d^1$ electron configuration is appropriate not only for the nine recently discovered Ln^{2+} ions in **2** but also for Dy^{2+} and Nd^{2+}, which traditionally have $4f^{n+1}$ electron configurations like Eu^{2+}, Yb^{2+}, Sm^{2+}, and Tm^{2+}. These results indicate that the ground state of a lanthanide ion in a molecule can be changed by the ligand set, a previously unknown option with these metals due to the limited radial extension of the 4f orbitals.
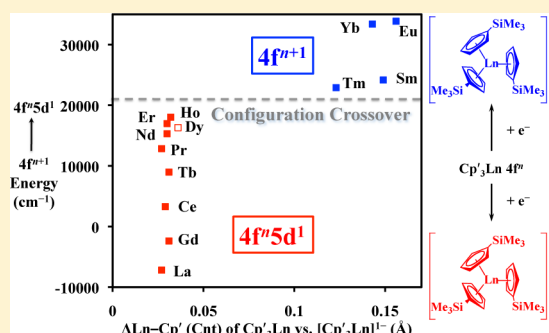
■ INTRODUCTION

For over 50 years, it was thought that only six lanthanide elements would form +2 ions. Eu^{2+}, Yb^{2+}, and Sm^{2+} were known since the 1920s in solution and in the solid state.[1-4] Tm^{2+}, Dy^{2+}, and Nd^{2+} were known only in the solid state[5-7] until 1997−2001 when the first solution examples were found.[8-14] The existence of just six Ln^{2+} ions was well justified on the basis of extensive solid state data and calculated redox potentials.[6,15-19] Solid state compounds formed under thermodynamic control at high temperature that contained +2 ions by stoichiometry, e.g., $LnX_{2,}$, were found to be $Ln^{2+}(X^{1-})_2$ salts only with Ln = Eu, Yb, Sm, Tm, Dy, and Nd. For the other lanthanides, the solids were best described as $Ln^{3+}(X^{1-})_2(e^{1-})$ materials with a delocalized electron in a conduction band;[16,20] i.e., Ln^{2+} did not form under these conditions. A "configuration crossover" was described for the difference between the six "pseudo-alkaline-earth lanthanides," i.e., Eu, Yb, Sm, Tm, Dy, and Nd, and the other lanthanides.[21]

A similar dichotomy was observed in solution based on calculated generic reduction potentials for conversion of a $4f^n$ Ln^{3+} ion to a $4f^{n+1}$ Ln^{2+} ion, Table 1. The calculated reduction potentials for the lanthanides beyond the traditional six Ln^{2+} ions known in the solid state were so negative, namely, −2.7 to

Table 1. Calculated Ln^{3+}/Ln^{2+} Reduction Potentials of Yttrium and the Lanthanides[17,22]

Ln	potential (V vs NHE)	Ln	potential (V vs NHE)
Eu	−0.35	Y	−2.8
Yb	−1.15	Pr	−2.9
Sm	−1.55	Ho	−2.9
Tm	−2.3	Er	−3.1
Dy	−2.5	La	−3.1
Nd	−2.6	Ce	−3.2
Pm	−2.7	Tb	−3.7
Lu	−2.7	Gd	−3.9

−3.9 V vs NHE [17] (−3.1 to −4.3 V vs Fc/Fc⁺),[23] that these ions would be expected to decompose all common solvents. Indeed, the high reactivity of even Dy^{2+} and Nd^{2+} with solvents suggested that the more reducing ions would be unstable in solution.[8-10,13,14,24-29]

However, it recently has been shown that Ln^{2+} ions are accessible for all of the lanthanides except Pm, which was not
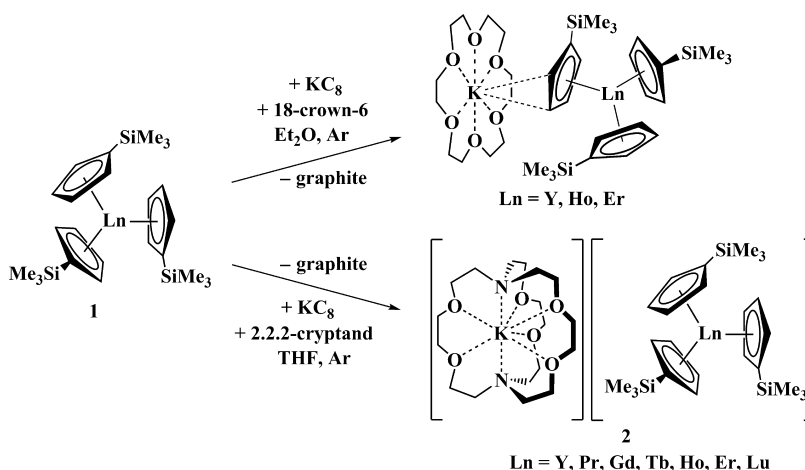
Scheme 1. Crystallographically Characterized Products of Reduction of Cp″$_3$Ln (Ln = La and Ce; Cp″ = C$_5$H$_3$(SiMe$_3$)$_2$-1,3) by Lappert et al.[30]
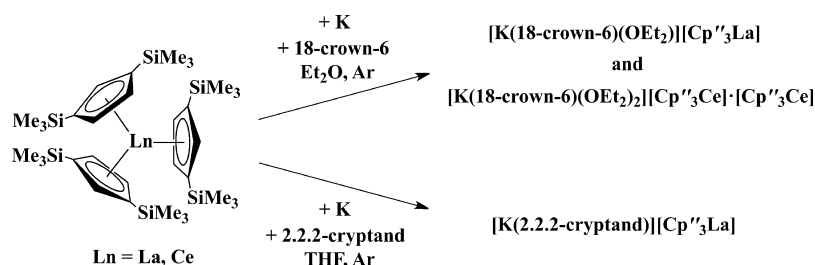
Scheme 2. Crystallographically Characterized Products of Reduction of Cp′$_3$Ln (Ln = Y, Pr, Gd, Tb, Ho, Er, Lu; Cp′ = C$_5$H$_4$SiMe$_3$)[31−33]

investigated because of its radioactivity. Complexes of nine new +2 ions, La^{2+}, Ce^{2+}, Pr^{2+}, Gd^{2+}, Tb^{2+}, Ho^{2+}, Er^{2+}, Y^{2+}, and Lu^{2+}, were synthesized via Schemes 1 and 2.[30−33] These new complexes had major structural differences compared to complexes of the traditional six +2 ions in that the difference in bond distances between a +2 ion complex and its +3 ion analog was small. Hence, all of the Ln^{2+} complexes in Schemes 1 and 2 have Ln−(cyclopentadienyl ring centroid) distances that are only 0.020−0.032 Å (∼1%) longer than their Ln^{3+} analogs. This contrasted so sharply with the 0.10−0.20 Å (∼6%) differences generally seen for complexes of Eu^{2+}, Yb^{2+}, Sm^{2+}, Tm^{2+}, Dy^{2+}, and Nd^{2+} compared to their Ln^{3+} counterparts[9,10,18,34−37] that there was initial skepticism that the new complexes contained +2 ions.

The large differences in bond distances between Ln^{2+} complexes of the traditional six Ln^{2+} lanthanides and their Ln^{3+} analogs are expected, since there are large differences between the radii of 4f^n Ln^{3+} and 4f^{n+1} Ln^{2+} ions and there is little metal−ligand interaction due to the contracted nature of the 4f orbitals. A typical example is that the average Sm−(C$_5$Me$_5$ centroid) and Sm−O distances in the Sm^{2+} complex (C$_5$Me$_5$)$_2$Sm(THF)$_2$ (2.599 and 2.633 Å, respectively)[38] are 0.176 and 0.173 Å longer than those in the compositionally similar Sm^{3+} compound [(C$_5$Me$_5$)$_2$Sm(THF)$_2$][BPh$_4$] (2.423 and 2.457 Å).[39] Another example pertinent to this study is the 2.486 Å average Sm−(Cp″ centroid) distance in the Sm^{3+} complex, Cp″$_3$Sm,[40] vs the 2.676 Å analog in [K(18-crown-6)(toluene)$_2$][Cp″$_3$Sm].[35]

The small differences in bond distances in the +2 vs +3 complexes in Schemes 1 and 2 were similar to the small changes with changing oxidation state observed in transition metal complexes.[41] In transition metal complexes, the bonding is not simply a sum of ionic radii because there are covalent interactions between the metal d orbitals and the ligands. Since spectroscopic and theoretical analyses indicated that the Ln^{2+} ions in Schemes 1 and 2 had 4f^{n}5d^1 and not 4f^{n+1} electron configurations (4d^1 for Y^{2+}), the small increases in bond distances could be explained by the d character in the configurations of the +2 ions. The accessibility of d^1 configurations for these ions was consistent with the crystal field splitting in the tris(cyclopentadienyl) ligand environment of these compounds.[42−47] In this trigonal field, the d$_{z^2}$ orbital is lowest in energy. Apparently, its energy is low enough with respect to the 4f orbitals that the d$_{z^2}$ orbital can be populated in the reduction reactions of Schemes 1 and 2.

Although a correlation existed between 4f^{n}5d^1 electron configuration and Ln^{3+}/Ln^{2+} size differences for the +2 ions in Schemes 1 and 2 vs the traditional six +2 ions with 4f^{n+1} configurations, the size comparisons were not made on the same set of complexes. Accordingly, it was of interest to make the [K(2.2.2-cryptand)][Cp′$_3$Ln] complexes, **2**, of the traditional six +2 ions, Eu^{2+}, Yb^{2+}, Sm^{2+}, Tm^{2+}, Dy^{2+}, and Nd^{2+}, for direct comparison with those in Scheme 2. To include comparisons with the Ln^{2+} ions found by Lappert, Scheme 1, using one uniform ligand set, the Ln = La and Ce versions of **2** were also synthesized. To make the Ln^{3+}/Ln^{2+} bond distance comparisons, the Cp′$_3$Ln complexes, **1**, of Eu, Yb, Sm, Tm, and Dy also had to be synthesized and structurally characterized.

These syntheses and crystallographic analyses allow the first comparison of all the lanthanides in the same coordination environment in both +2 and +3 oxidation states. The results are described here along with a comparison of UV−vis spectra of

the analogous complexes of the traditional six Ln^{2+} ions vs all the other Ln^{2+} ions in the series. The density functional theory (DFT) analysis of the structural and spectroscopic data have proven very valuable in understanding the results and are also reported.

■ EXPERIMENTAL SECTION

The syntheses and manipulations described below were conducted under argon with rigorous exclusion of air and water using glovebox, vacuum line, and Schlenk techniques. Solvents were sparged with UHP grade argon (Airgas) and passed through columns containing Q-5 and molecular sieves before use. NMR solvents (Cambridge Isotope Laboratories) were dried over NaK/benzophenone, degassed by three freeze−pump−thaw cycles, and vacuum-transferred before use. Anhydrous $LnCl_3$ (Ln = La, Ce, Nd, Sm, Dy, Yb),[48] $LnI_2(THF)_2$ (Ln = Eu, Yb),[49,50] $TmI_3(THF)_{3.5}$,[51] KC_8,[52] $AgBPh_4$,[53] KCp'[54] and Cp'_3Ln, **1-Ln** (Ln = La,[54] Ce,[55,56] Nd[57]), were prepared according to literature. 2.2.2-Cryptand, 4,7,13,16,21,24-hexaoxa-1,10-diazabicyclo[8.8.8]hexacosane (Acros Organics), was placed under vacuum (10^{-3} Torr) for 12 h before use. ^{1}H NMR (500 MHz) and ^{13}C NMR (125 MHz) spectra were obtained on a Bruker GN500 or CRYO500 MHz spectrometer at 298 K. For some paramagnetic compounds, ^{1}H NMR spectra could only be observed when a capillary tube containing pure deuterated solvent was placed in the paramagnetic solution to assist in properly locking and shimming the instrument. IR samples were prepared as KBr pellets, and the spectra were obtained on a Varian 1000 FT-IR spectrometer. Elemental analyses were performed on a PerkinElmer 2400 series II CHNS elemental analyzer. EPR spectra were collected using X-band frequency (9.3−9.8 GHz) on a Bruker EMX spectrometer equipped with an ER041XG microwave bridge, and the magnetic field was calibrated with DPPH (g = 2.0036). UV−vis spectra were obtained in THF at 298 K using a Varian Cary 50 Scan UV−vis spectrophotometer.

[K(2.2.2-cryptand)][Cp'$_3$La], 2-La. In an argon-filled glovebox, Cp'_3La, **1-La** (208 mg, 0.378 mmol), and 2.2.2-cryptand (142 mg, 0.377 mmol) were combined and dissolved in THF (2 mL). KC_8 (75 mg, 0.55 mmol) was quickly added to the stirred colorless solution. The reaction mixture immediately turned black/violet, and after 1 min of stirring, Et_2O (3 mL) was added and the mixture was filtered to remove a black precipitate, presumably graphite. The dark purple filtrate was cooled to −35 °C in the freezer for 1 h. The solution was layered with additional Et_2O (15 mL) and stored at −35 °C for 24 h to produce a black/purple crystalline solid. The mother liquor was decanted and the solids were rinsed with Et_2O (2 mL) and briefly dried under vacuum to yield **2-La** as a black/purple crystalline solid that analyzed as the solvate $[K(2.2.2\text{-cryptand})][Cp'_3La]\cdot THF$ (230 mg, 59%). Black/purple single crystals of **2-La·THF**, suitable for X-ray diffraction, were grown from THF/Et_2O at −35 °C. IR: 3069m, 2946s, 2887s, 2820m, 1925w, 1577w, 1480m, 1447m, 1433m, 1405w, 1354s, 1301m, 1260m, 1237s, 1172s, 1135s, 1105s, 1082s, 1034s, 949s, 932m, 901s, 832s, 745s, 729m, 688w, 673m, 626m cm^{-1}. Anal. Calcd for $C_{42}H_{75}N_2O_6Si_3KLa\cdot C_4H_8O$: C, 53.21; H, 8.06; N, 2.70. Found: C, 52.83; H, 8.44; N, 2.74. UV−vis (THF) λ_{max}, nm (ε, M^{-1} cm^{-1}): 310 (4400), 433 (3900 shoulder), 502 (5600 shoulder), 554 (6500), 692 (2600 shoulder).

[K(2.2.2-cryptand)][Cp'$_3$Ce], 2-Ce. As described for **2-La**, bright blue solids of **1-Ce** (189 mg, 0.342 mmol) and 2.2.2-cryptand (129 mg, 0.343 mmol) were dissolved in THF (2 mL) to form an amber solution, which was combined with KC_8 (65 mg, 0.48 mmol) to produce **2-Ce** as a black/purple crystalline solid that analyzed as the solvate $[K(2.2.2\text{-cryptand})][Cp'_3Ce]\cdot THF$ (188 mg, 53%). Black/purple single crystals of **2-Ce·THF**, suitable for X-ray diffraction, were grown from THF/Et_2O at −35 °C. IR: 3070w, 2946s, 2888s, 2821m, 2486w, 1585w, 1480m, 1447m, 1434m, 1405w, 1355s, 1301m, 1260m, 1237s, 1172s, 1135s, 1107s, 1081s, 1035s, 950m, 932m, 901s, 832s, 746s, 730m, 673w, 626m cm^{-1}. Anal. Calcd for $C_{42}H_{75}N_2O_6Si_3KCe\cdot C_4H_8O$: C, 53.14; H, 8.05; N, 2.69. Found: C, 52.94; H, 8.37; N, 2.73.

UV−vis (THF) λ_{max}, nm (ε, M^{-1} cm^{-1}): 385 (3800), 462 (4000 shoulder), 538 (4500), 635 (4700).

[K(2.2.2-cryptand)][Cp'$_3$Nd], 2-Nd. As described for **2-La**, dull green solids of **1-Nd** (206 mg, 0.370 mmol) and 2.2.2-cryptand (140 mg, 0.372 mmol) were dissolved in THF (2 mL) to form a light aquamarine-purple solution, which was combined with KC_8 (71 mg, 0.52 mmol) to produce **2-Nd** as a black/maroon-purple crystalline solid that analyzed as the solvate $[K(2.2.2\text{-cryptand})][Cp'_3Nd]\cdot THF$ (106 mg, 27%). Black/maroon-purple single crystals of **2-Nd·THF**, suitable for X-ray diffraction, were grown from THF/Et_2O at −35 °C. IR: 3072m, 2946s, 2888s, 2824m, 2362w, 1925s, 1589w, 1480m, 1447m, 1435m, 1354s, 1301m, 1260m, 1236s, 1174s, 1135s, 1107s, 1082s, 1036s, 950s, 932m, 902s, 832s, 747s, 674w, 631m cm^{-1}. Anal. Calcd for $C_{42}H_{75}N_2O_6Si_3KNd\cdot C_4H_8O$: C, 52.93; H, 8.02; N, 2.68. Found: C, 52.58; H, 8.31; N, 2.71. UV−vis (THF) λ_{max}, nm (ε, M^{-1} cm^{-1}): 420 (4700), 483 (4200 shoulder), 654 (2000 shoulder).

Cp'$_3$Sm, 1-Sm. In an argon-filled glovebox, a sealable 100 mL side arm Schlenk flask equipped with a greaseless stopcock was charged with $SmCl_3$ (286 mg, 1.11 mmol), a magnetic stir bar, and Et_2O (20 mL). A solution of KCp' (600 mg, 3.40 mmol) in Et_2O (20 mL) was added to the stirred slurry, and the mixture was stirred at room temperature for 12 h. The solvent was removed under vacuum from the resulting yellow mixture. Hexane (40 mL) was added to the reaction flask. The flask was attached to a Schlenk line, and the mixture was heated to reflux for 6 h. The solvent was removed under vacuum, and the flask was brought into a glovebox free of coordinating solvents. Additional hexane (30 mL) was added, and the resulting light orange suspension was filtered to remove white solids, presumably KCl and excess KCp'. The solvent was removed from the filtrate under vacuum. The resulting bright orange solids were extracted with pentane (10 mL), and removal of solvent under vacuum afforded **1-Sm** as a microcrystalline bright orange solid (525 mg, 84%). Bright orange single crystals of **1-Sm**, suitable for X-ray diffraction, were grown from pentane at −35 °C. ^{1}H NMR (C_6D_6): δ 22.28 (s, $C_5H_4SiMe_3$, 6H), 13.15 (s, $C_5H_4SiMe_3$, 6H), −3.69 (s, $C_5H_4SiMe_3$, 27H). IR: 3064w, 2953m, 2895m, 2714w, 2361w, 1872w, 1847w, 1745w, 1577m, 1442m, 1411w, 1364m, 1312w, 1243s, 1196w, 1178s, 1061w, 1042s, 998w, 903s, 832s, 773s, 750s, 685m, 631m cm^{-1}. Anal. Calcd for $C_{24}H_{39}Si_3Sm$: C, 51.27; H, 6.99. Found: C, 51.02; H, 6.67.

[K(2.2.2-cryptand)][Cp'$_3$Sm], 2-Sm. As described for **2-La**, a light orange solution of **1-Sm** (191 mg, 0.340 mmol) and 2.2.2-cryptand (128 mg, 0.340 mmol) in THF (2 mL) was combined with KC_8 (50 mg, 0.37 mmol) to produce **2-Sm** as a dark purple crystalline solid that analyzed as the solvate $[K(2.2.2\text{-cryptand})][Cp'_3Sm]\cdot THF$ (171 mg, 48%). Dark purple single crystals of **2-Sm·THF**, suitable for X-ray diffraction, were grown from THF/Et_2O at −35 °C. IR: 3337w, 3270w, 3068m, 2948s, 2891s, 2824w, 2349w, 2086w, 1570w, 1480m, 1438s, 1354s, 1302m, 1260s, 1240s, 1183s, 1135s, 1107s, 1082s, 1035s, 950m, 932m, 904s, 832s, 737s, 677m, 628m cm^{-1}. Anal. Calcd for $C_{42}H_{75}N_2O_6Si_3KSm\cdot C_4H_8O$: C, 52.62; H, 7.97; N, 2.67. Found: C, 52.49; H, 8.34; N, 2.64. UV−vis (THF) λ_{max}, nm (ε, M^{-1} cm^{-1}): 360 (700), 402 (500), 509 (600), 566 (400 shoulder), 680 (200).

Cp'$_2$Eu(THF)$_2$, 3-Eu. In an argon-filled glovebox, a solution of KCp' (368 mg, 2.09 mmol) in THF (6 mL) was added to a stirred pale yellow-green slurry of $EuI_2(THF)_2$ (560 mg, 1.02 mmol). The mixture immediately turned bright orange. After 2 h of stirring, the mixture was centrifuged to remove white solids, presumably KI, and the bright red-orange supernatant was stirred while hexane (5 mL) was added slowly. The white solids that precipitated were removed via filtration, and the filtrate was concentrated to 1 mL under reduced pressure. The thick oil was layered with Et_2O (15 mL) and stored at −35 °C for 2 d, which produced red-orange crystals that were suitable for X-ray diffraction. The mother liquor was decanted and the crystals were dried under vacuum to yield **3-Eu** as a bright red-orange solid (404 mg, 69%). IR: 3083w, 3058w, 2951m, 2888m, 2699w, 2361w, 1868w, 1558w, 1440m, 1398w, 1354m, 1306w, 1244s, 1182w, 1106w, 1038w, 904s, 834s, 793m, 776s, 762s, 749s, 685w, 641m, 629m cm^{-1}. Anal. Calcd for $C_{16}H_{26}Si_2Eu$: C, 45.06; H, 6.14. Found: C, 44.93; H, 6.09.

[K(2.2.2-cryptand)][Cp′₃Eu], 2-Eu. In an argon-filled glovebox, a solution of KCp′ (31 mg, 0.18 mmol) and 2.2.2-cryptand (66 mg, 0.18 mmol) in THF (1 mL) was added to a stirred solution of Cp′₂Eu(THF)₂, **3-Eu** (100 mg, 0.175 mmol), in THF (1 mL). An immediate color change from bright red-orange to dark magenta-purple resulted. After 5 min of stirring, the solution was concentrated to ∼0.5 mL under reduced pressure, layered with Et₂O (6 mL), and stored at −35 °C for 2 d to produce dark purple crystals, suitable for X-ray diffraction. The mother liquor was decanted and the crystals were briefly dried under vacuum to yield **2-Eu** as a dark purple crystalline solid that analyzed as the solvate [K(2.2.2-cryptand)]-[Cp′₃Eu]·THF (150 mg, 82%). Dark purple single crystals of **2-Eu·THF**, suitable for X-ray diffraction, were grown from THF/Et₂O at −35 °C. IR: 3068w, 2948s, 2892s, 2825m, 1480w, 1447m, 1438m, 1361s, 1354s, 1302m, 1259m, 1239s, 1183m, 1135s, 1105s, 1082s, 1035s, 950s, 932m, 904s, 832s, 746s, 687w, 677w, 639w, 628m cm⁻¹. Anal. Calcd for C₄₂H₇₅N₂O₆Si₃KEu·C₄H₈O: C, 52.54; H, 7.79; N, 2.61. Found: C, 52.43; H, 7.98; N, 2.62. UV−vis (THF) λ$_{max}$, nm (ε, M⁻¹ cm⁻¹): 483 (300), 559 (200 shoulder).

Cp′₃Eu, 1-Eu. In an argon-filled glovebox, AgBPh₄ (191 mg, 0.447 mmol) was added to a stirred dark magenta-purple solution of [K(2.2.2-cryptand)][Cp′₃Eu]·THF, **2-Eu** (427 mg, 0.406 mmol), in THF (10 mL). Within 1 min of stirring, the mixture became dark black/red in color. Black solids, presumably Ag⁰, were removed via filtration, and the solvent was removed under vacuum. The tacky residue was stirred in hexane (10 mL) for 30 min, filtered to remove a white solid, presumably [K(2.2.2-cryptand)][BPh₄], and the solvent was removed under vacuum. Several cycles of dissolution in hexane and removal of solvent yielded **1-Eu** as a dark red microcrystalline solid (183 mg, 80%). Dark red crystals of **1-Eu**, suitable for X-ray diffraction, were grown from a concentrated pentane solution at −35 °C. ¹H NMR (C₆D₆): δ 53.32 (br s, C₅H₄Si*Me*₃, 27H), 47.60 (br s, C₅H₄Si*Me*₃, 6H), −26.25 (br s, C₅H₄Si*Me*₃, 6H). IR: 3063m, 2953m, 2895w, 2807w, 2361w, 1744w, 1444w, 1405w, 1361m, 1311w, 1243m, 1193w, 1177m, 1044w, 903m, 884w, 833s, 792m, 771s, 751s, 685m, 631m, 533s cm⁻¹. Anal. Calcd for C₂₄H₃₉Si₃Eu: C, 51.13; H, 6.97. Found: C, 51.24; H, 6.97.

Cp′₃Dy, 1-Dy. As described for **1-Sm**, in an argon-filled glovebox, DyCl₃ (492 mg, 1.83 mmol) and KCp′ (1.00 g, 5.67 mmol) were combined to produce **1-Dy** as a microcrystalline bright yellow solid (906 mg, 86%). Bright yellow single crystals of **1-Dy**, suitable for X-ray diffraction, were grown from pentane at −35 °C. ¹H NMR (C₆D₆): δ 141 (br s, C₅H₄Si*Me*₃, 6H), −216 (br s, C₅H₄Si*Me*₃, 27H). IR: 3966w, 3914w, 3554w, 3471w, 3067w, 2953m, 2895m, 2717w, 2619w, 2422w, 2385w, 2349w, 2284w, 2233w, 2080w, 1997w, 1932w, 1873w, 1782w, 1753, 1655w, 1555w, 1443m, 1414m, 1400m, 1366m, 1313m, 1243s, 1198m, 1178s, 1063m, 1042m, 904s, 869s, 834s, 796s, 776s, 752s, 685m, 631m cm⁻¹. Anal. Calcd for C₂₄H₃₉Si₃Dy: C, 50.19; H, 6.84. Found: C, 49.79; H, 6.74.

[K(2.2.2-cryptand)][Cp′₃Dy], 2-Dy. As described for **2-La**, a light yellow solution of **1-Dy** (158 mg, 0.275 mmol) and 2.2.2-cryptand (103 mg, 0.274 mmol) in THF (2 mL) was combined with KC₈ (52 mg, 0.38 mmol) to produce **2-Dy** as a black/dark maroon-purple crystalline solid that analyzed as the solvate [K(2.2.2-cryptand)]-[Cp′₃Dy]·THF (124 mg, 43%). Dark purple/green single crystals of **2-Dy·THF**, suitable for X-ray diffraction, were grown from THF/Et₂O at −35 °C. IR: 3078w, 2947m, 2888s, 2825m, 2360w, 1480w, 1447w, 1354m, 1301w, 1260m, 1236m, 1176m, 1135s, 1105s, 1082s, 1036s, 950m, 932w, 903m, 831s, 751m, 673w, 626w cm⁻¹. Anal. Calcd for C₄₂H₇₅N₂O₆Si₃KDy·C₄H₈O: C, 52.02; H, 7.88; N, 2.64. Found: C, 51.92; H, 8.22; N, 2.63. UV−vis (THF) λ$_{max}$, nm (ε, M⁻¹ cm⁻¹): 483 (3400), 644 (1000 shoulder).

Cp′₃Tm, 1-Tm. As described for **1-Sm**, in an argon-filled glovebox, TmI₃(THF)₃.₅ (743 mg, 0.926 mmol) and KCp′ (502 mg, 2.85 mmol) were combined to produce **1-Tm** as a microcrystalline bright yellow solid (510 mg, 95%). Bright yellow single crystals of **1-Tm**, suitable for X-ray diffraction, were grown from pentane at −35 °C. ¹H NMR (C₆D₆): δ 153.9 (s, C₅H₄Si*Me*₃, 27H), −32.8 (br s, C₅H₄Si*Me*₃, 6H), −454 (br s, C₅H₄Si*Me*₃, 6H). IR: 3077w, 2953w, 2895w, 2716w, 2361w, 1934w, 1873w, 1760w, 1662w, 1566w, 1443m, 1414w, 1366m,

1314m, 1243s, 1197w, 1178m, 1064m, 1043s, 905m, 834s, 798s, 782s, 752s, 686m, 632m, 564w, 531w cm⁻¹. Anal. Calcd for C₂₄H₃₉Si₃Tm: C, 49.63; H, 6.77. Found: C, 49.64; H, 7.04.

[K(2.2.2-cryptand)][Cp′₃Tm], 2-Tm. As described for **2-La**, a light yellow solution of **1-Tm** (258 mg, 0.444 mmol) and 2.2.2-cryptand (167 mg, 0.444 mmol) in THF (2 mL) was combined with KC₈ (79 mg, 0.58 mmol) to produce **2-Tm** as a black/brown crystalline solid that analyzed as the solvate [K(2.2.2-cryptand)]-[Cp′₃Tm]·THF (313 mg, 66%). Dark brown single crystals of **2-Tm·THF**, suitable for X-ray diffraction, were grown from THF/Et₂O at −35 °C. IR: 3076w, 2948m, 2890s, 2825m, 2764w, 2731w, 2360w, 2341w, 1480w, 1447m, 1382m, 1397w, 1361m, 1354s, 1302m, 1259m, 1240s, 1182m, 1135s, 1105s, 1082s, 1035s, 950m, 932w, 905m, 833s, 748s, 735s, 687w, 677w, 630w, 552w cm⁻¹. Anal. Calcd for C₄₂H₇₅N₂O₆Si₃KTm·C₄H₈O: C, 51.71; H, 7.83; N, 2.62. Found: C, 51.32; H, 8.27; N, 2.64. UV−vis (THF) λ$_{max}$, nm (ε, M⁻¹ cm⁻¹): 416 (600), 550 (400), 634 (300 shoulder), 794 (100 shoulder).

Cp′₃Yb, 1-Yb. As described for **1-Sm**, in an argon-filled glovebox, YbCl₃ (751 mg, 2.72 mmol) and KCp′ (1.52 g, 8.62 mmol) were combined to produce **1-Yb** as a microcrystalline forest green solid (338 mg, 22%). Before the pentane extraction, a significant amount of red solids were observed and identified as [Cp′₂Yb(μ-Cl)]₂ through X-ray diffraction.⁵⁸ Dark green single crystals of **1-Yb**, suitable for X-ray diffraction, were grown from pentane at −35 °C. ¹H NMR (C₆D₆): δ 44.2 (s, C₅H₄Si*Me*₃, 27H), 43.8 (s, C₅H₄Si*Me*₃, 6H), −21.5 (br s, C₅H₄Si*Me*₃, 6H). IR: 2954m, 2895w, 2388w, 2236w, 2086w, 1933w, 1760w, 1663w, 1568w, 1527w, 1444m, 1410w, 1365m, 1313w, 1244s, 1198m, 1177s, 1063m, 1044s, 906s, 834s, 778s, 752s, 686m, 631m cm⁻¹. Anal. Calcd for C₂₄H₃₉Si₃Yb: C, 49.29; H, 6.72 Found: C, 48.65; H, 6.69.

Cp′₂Yb(THF)₂, 3-Yb. As described for **3-Eu**, in an argon-filled glovebox, YbI₂(THF)₂ (790 mg, 1.38 mmol) and KCp′ (500 mg, 2.83 mmol) were combined to produce **3-Yb** as a dark purple diamagnetic solid as identified by ¹H NMR spectroscopy⁵⁸ (679 mg, 83%).

[K(2.2.2-cryptand)][Cp′₃Yb], 2-Yb. As described for **2-Eu**, in an argon-filled glovebox, Cp′₂Yb(THF)₂, **3-Yb** (664 mg, 1.12 mmol), 2.2.2-cryptand (423 mg, 1.12 mmol), and KCp′ (200 mg, 1.13 mmol) were combined to produce **2-Yb·THF** as emerald green crystals that were suitable for X-ray diffraction (906 mg, 75%). ¹H NMR (THF-d₈): δ 5.93 (s, C₅H₄SiMe₃, 6H), 5.73 (s, C₅H₄SiMe₃, 6H), 3.51 (s, OCH₂CH₂O, 12H), 3.48 (t, ³J$_{HH}$ = 4.5 Hz, NCH₂CH₂O, 12H), 2.50 (t, ³J$_{HH}$ = 4.5 Hz, NCH₂CH₂O, 12H), 0.14 (s, C₅H₄SiMe₃, 27H). ¹³C NMR (C₆D₆): δ 117.0 (C₅H₄SiMe₃), 110.7 (C₅H₄SiMe₃), 109.2 (C₅H₄SiMe₃), 71.3 (OCH₂CH₂O), 68.4 (NCH₂CH₂O), 54.8 (NCH₂CH₂O), 1.6 (C₅H₄SiMe₃). IR: 3075w, 2949m, 2890m, 2826m, 1480w, 1438m, 1354s, 1302m, 1259m, 1240s, 1183m, 1135s, 1105s, 1081s, 1035s, 945s, 932m, 905s, 832s, 738s, 677m, 638m, 630m, 571m cm⁻¹. Anal. Calcd for C₄₂H₇₅N₂O₆Si₃KYb·C₄H₈O: C, 51.51; H, 7.80; N, 2.61. Found: C, 51.13; H, 7.81; N, 2.47. UV−vis (THF) λ$_{max}$, nm (ε, M⁻¹ cm⁻¹): 335 (900 shoulder), 378 (800), 534 (50), 684 (200).

X-ray Data Collection, Structure Determination, and Refinement. Crystallographic details for compounds **2-La**, **2-Ce**, **2-Nd**, **1-Sm**, **2-Sm**, **1-Eu**, **2-Eu**, **1-Dy**, **2-Dy**, **1-Tm**, **2-Tm**, **1-Yb**, and **2-Yb** are summarized in the Supporting Information. **1-Ln** complexes for all the lanthanides (except unknown Pm) are isomorphous, as are all the complexes in the series **2-Ln**.

Computational Details. Density functional theory (DFT) calculations were carried out on **1-Ln** and the anion of **2-Ln** for Ln = Nd, Sm, Eu, Dy, Tm, and Yb using the hybrid meta-generalized gradient approximation functional TPSSH.⁵⁹,⁶⁰ All computations were performed using the TURBOMOLE program package.⁶¹ Small-core effective core potentials (ECPs),⁶² along with triple-ζ basis sets (def-TZVP),⁶³ were employed for heavy atoms, and augmented polarized split-valence basis sets (def2-SVPD)⁶⁴ were employed for light atoms. Solvation effects were taken into account through the continuum solvation model (COSMO)⁶⁵ using the dielectric constant of THF (ε = 7.520).⁶⁶ Time dependent DFT (TDDFT)⁶⁷ calculations were performed to simulate the UV−vis spectrum of **2**. A full description of the computational methods is supplied in the Supporting Information.

■ RESULTS

Synthesis of Cp′₃Ln (Ln = Sm, Dy, Tm). The synthesis of the previously unknown Cp′₃Ln complexes, **1** (Ln = Sm, Eu, Dy, Tm, Yb), needed as precursors in this study and for structural comparison, was attempted following the published syntheses of analogs of the other metals.[31−33,54−57] For Ln = Sm and Dy, the reaction of 3 equiv of KCp′ with LnCl₃ generated the desired bright orange Cp′₃Sm, **1-Sm**, and bright yellow Cp′₃Dy, **1-Dy**, Scheme 3. Since the analogous metal

Scheme 3. Routes for Synthesizing Cp′₃Ln Compounds, 1, from Lanthanide Trihalide Starting Materials
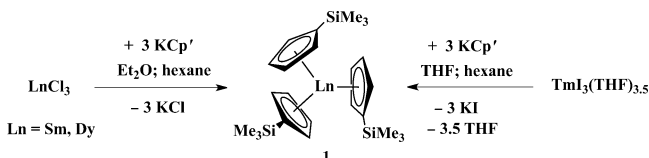
trichloride reaction was not as successful with thulium, bright yellow Cp′₃Tm, **1-Tm**, was prepared from the iodide precursor, TmI₃(THF)₃.₅,[51] with 3 equiv of KCp′, Scheme 3. **1-Sm**, **1-Dy**, and **1-Tm** were characterized by X-ray crystallography (see Supporting Information) and were found to be isomorphous with the other **1-Ln** complexes.[31−33,54−57]

Synthesis of Cp′₃Ln (Ln = Eu, Yb) and [K(2.2.2-cryptand)][Cp′₃Ln] (Ln = Eu, Yb). Attempts to make Cp′₃Eu, **1-Eu**, from EuCl₃ according to Scheme 1 were not successful. This was not unexpected, since it is known that the reaction of 3 equiv of NaC₅Me₅ with EuCl₃ resulted in the isolation of the Eu²⁺ complex (C₅Me₅)₂Eu(THF) rather than (C₅Me₅)₃Eu.[68] Similarly, the reaction of EuCl₃ with 2 equiv of KCpᴿ [Cpᴿ = C₅H₄CH(SiMe₃)₂] to make Cpᴿ₂EuCl yielded only the Eu²⁺ complex, Cpᴿ₂Eu(THF)₂.[27] This preference to form +2 complexes for europium and ytterbium is attributed to stabilization due to the half-filled and completely filled 4f electron configurations, 4f⁷ and 4f¹⁴, respectively, and the concomitant low reduction potentials, Table 1. To circumvent these problems, a reverse approach was used involving first the synthesis of the +2 complexes, **2**, and then subsequent oxidation to form the +3 compounds, **1**, needed for structural comparison.

Both EuI₂(THF)₂[50] and YbI₂(THF)₂[49] react with 2 equiv of KCp′ to produce Cp′₂Eu(THF)₂, **3-Eu**, and Cp′₂Yb(THF)₂, **3-Yb**, as bright orange-red and purple crystalline solids, respectively, eq 1. Complex **3-Yb** had been previously
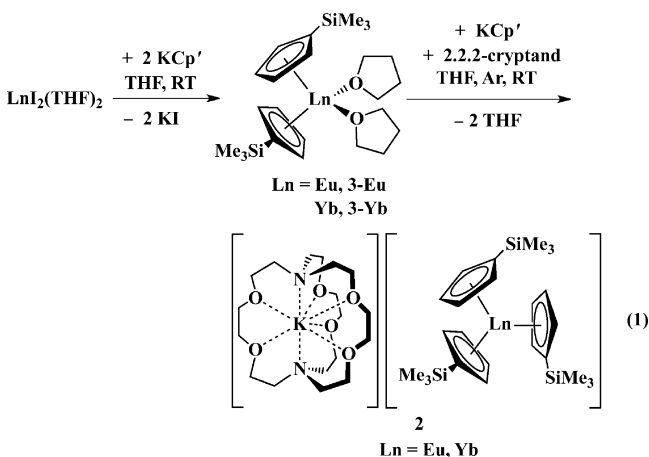
synthesized by Na(Hg) reduction of [Cp′₂Yb(μ-Cl)]₂, and its identity was verified by ¹H NMR spectroscopy.[58] Although **3-Eu** was too paramagnetic to be observed by NMR, single-crystal X-ray diffraction confirmed its composition and structure. The structure of **3-Eu** is isomorphous with **3-Yb**, but the low quality data precluded a detailed structural discussion.

To obtain the desired [K(2.2.2-cryptand)][Cp′₃Ln] products, **2-Eu** and **2-Yb**, K(2.2.2-cryptand)Cp′ was added to **3-Eu** and **3-Yb**, eq 1. Lappert reported a similar reaction in 1998 involving Cp″₂Sm, KCp″, and 18-crown-6 to make [K(18-crown-6)(toluene)₂][Cp″₃Sm] [Cp″ = C₅H₃(SiMe₃)₂].[35] Purple **2-Eu** and emerald **2-Yb** were characterized by X-ray crystallography (Figure 1), IR spectroscopy, and elemental
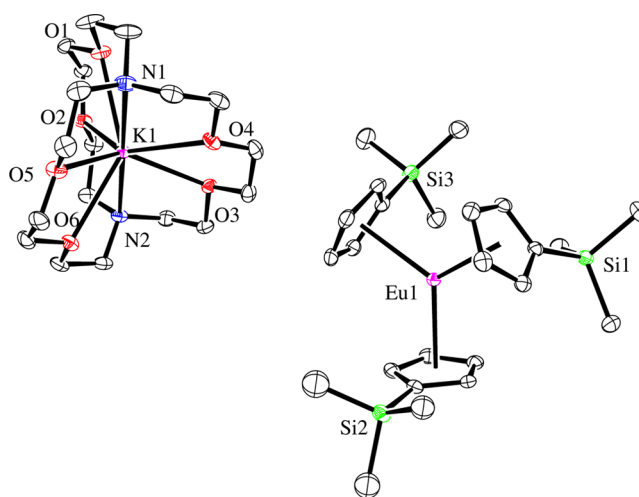
Figure 1. Molecular structure of [K(2.2.2-cryptand)][Cp′₃Eu], **2-Eu**, with thermal ellipsoids drawn at the 50% probability level. One set of disordered carbons in a disordered trimethylsilyl group, a disordered cocrystallized THF, and hydrogen atoms are omitted for clarity.

analysis. Complex **2-Yb** exhibited a ¹H NMR spectrum that was characteristic of a diamagnetic compound, which is consistent with its electron configuration being 4f¹⁴ and not 4f¹³5d¹.

The Eu³⁺ complex, Cp′₃Eu, **1-Eu**, needed for structural comparison was made by oxidation of [K(2.2.2-cryptand)]-[Cp′₃Eu], **2-Eu**, with AgBPh₄. The dark red product was identified by X-ray crystallography, elemental analysis, and IR spectroscopy, eq 2. The Yb³⁺ analog, **1-Yb**, was also synthesized

(1)

2
Ln = Eu, Yb

(2)

1
Ln = Eu, Yb
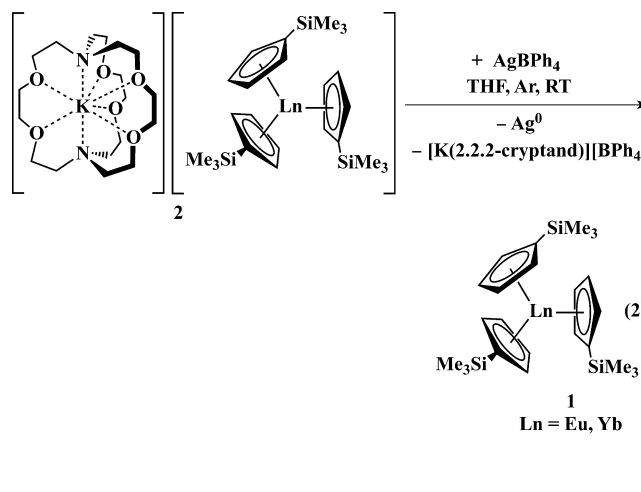
by the oxidation of [K(2.2.2-cryptand)][Cp$'_3$Yb], **2-Yb**, with AgBPh$_4$ and identified by X-ray crystallography, eq 2. The green **1-Yb** can also be synthesized by reacting 3 equiv of KCp$'$ with YbCl$_3$, Scheme 3, although the latter reaction produced significant amounts of the known byproduct, [Cp$'_2$Yb(μ-Cl)]$_2$.[69]

Synthesis of [K(2.2.2-cryptand)][Cp$'_3$Ln], 2 (Ln = La, Ce, Nd, Sm, Dy, Tm). Following the procedure previously reported for Ln = Pr, Gd, Tb, Y, Ho, Er, and Lu,[33] which required short reaction times and fast isolation procedures, the Cp$'_3$Ln complexes **1-La**, **1-Ce**, **1-Nd**, **1-Sm**, **1-Dy**, and **1-Tm** were reacted with KC$_8$ in the presence of 2.2.2-cryptand in THF under argon. These reactions yielded deeply colored crystalline products, all of which were determined by X-ray crystallography to be [K(2.2.2-cryptand)][Cp$'_3$Ln], **2**, eq 3.

$$\text{1} \quad \xrightarrow[\text{– graphite}]{\substack{+ \text{ KC}_8 \\ + \text{ 2.2.2-cryptand} \\ \text{THF, Ar, RT}}} \tag{3}$$

Ln = La, Ce, Nd, Sm, Dy, Tm
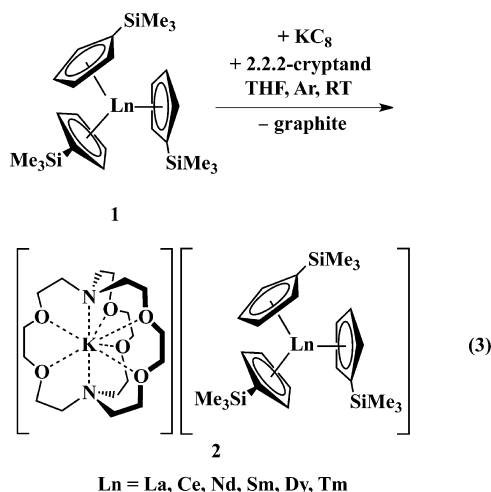
The lanthanum complex, **2-La**, displays an isotropic EPR spectrum, Figure 2, that is very similar to the La^{2+} spectra
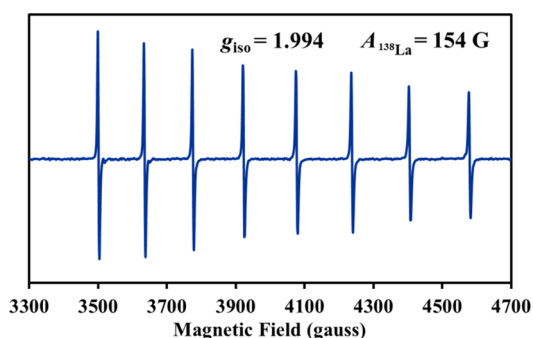
Figure 2. Room temperature X-band EPR spectrum of [K(2.2.2-cryptand)][Cp$'_3$La], **2-La**, in THF under argon.

reported for the [Cp$''_3$La]$^{1-}$ anion by Lappert et al.[30,70] The octet pattern is evidence of an unpaired electron coupled to the $I = {}^7/_2$ nuclear spin of ^{138}La (99.9% natural abundance). The large average coupling constant of 154 G and the g_{iso} value of 1.994 (similar to the 133.5 G and g_{av} = 1.990 of [Cp$''_3$La]$^{1-}$) are both indicative of a metal-centered radical and consistent with the 5d^1 configuration assigned to La^{2+}.[30] These EPR data can also be compared to the data on the 6d^1 Th^{3+} complexes, [C$_5$H$_3$(SiMe$_3$)$_2$-1,3]$_3$Th,[71,72] [C$_5$H$_3$(SiMe$_2^t$Bu)$_2$-1,3]$_3$Th,[71] (C$_5$Me$_5$)$_2$[^{i}PrNC(Me)N^{i}Pr]Th,[73] [K(DME)$_2$]-

{[C$_8$H$_6$(Si^{t}BuMe$_2$)$_2$]$_2$Th},[74] and (C$_5$Me$_4$H)$_3$Th[75] that have EPR spectra with g values of 1.87–1.92.

Structural Comparisons. Crystallographic information was obtained on the Ln^{3+} complexes **1** (Sm, Eu, Dy, Tm, and Yb) to complement that already in the literature (La,[54] Ce,[55,56] Nd[57]) so that a direct structural comparison of **1** and **2** could be made for these metals to add to the data already available on the other metals in the series.[33] The differences between the Ln–(Cp$'$ centroid) distances of **1** and **2** for Ln = La and Ce, 0.027 and 0.029 Å, respectively, match the small differences observed between **1** and **2** for the Ln^{2+} ions in Scheme 2 where Ln = Y,[31] Ho,[32] Er,[32] Tb,[33] Pr,[33] Gd,[33] Lu[33] (0.027–0.032 Å) and between Scheme 1 complexes Cp$''_3$La and [Cp$''_3$La]$^{1-}$ (0.020–0.032 Å).[30] These small changes in bond length are typical in transition metal chemistry[41] and are consistent with the assignment of a 4f^{n}5d^1 configuration rather than a 4f^{n+1} configuration for the +2 ions of these lanthanide metals. The 5d^1 configuration has previously been assigned[30] to La^{2+} in [Cp$''_3$Ln]$^{1-}$, and yttrium necessarily has a 4d^1 configuration.

In contrast to these small differences, the differences in Ln–(Cp$'$ centroid) distances of **1** and **2** for *four of the traditional six* divalent lanthanides are larger: 0.156 Å (Eu), 0.143 Å (Yb), 0.147 Å (Sm), and 0.123 Å (Tm) (Table 2, listed in the order of increasingly negative Ln^{3+}/Ln^{2+} reduction potentials in Table 1). These larger values match the 0.10–0.20 Å differences found historically for metal–ligand bonds in Ln^{2+} complexes of Eu, Yb, Sm, Tm, Dy, and Nd[9,10,18,34–37] when compared to their Ln^{3+} analogs. These four 0.123–0.156 Å differences in Ln–(Cp$'$ centroid) distances between **1** and **2** are consistent with those expected for a 4f^{n+1} Ln^{2+} complex vs a 4f^n Ln^{3+} species. This consistently large difference is attributed to the special nature of the 4f orbitals and their limited radial extension that minimizes metal ligand interaction and causes these complexes to behave more as complexes of "free ions" rather than as d-block complexes. Both the spectroscopy and magnetism of complexes of these traditional Ln^{2+} ions support this free ion view.[16,17,76–81]

Although four of the traditional six Ln^{2+} ions in complexes of **2** have large Ln–(Cp$'$ centroid) distances compared to the Ln^{3+} analogs, **1**, complexes of Dy^{2+} and Nd^{2+} do not (Table 2). The Ln^{3+}/Ln^{2+} difference between **1** and **2** for Dy is 0.036 Å and for Nd is 0.030 Å. This puts these two metals in the same category as the metals that are expected to have 4f^{n}5d^1 configurations in the +2 oxidation state. Hence, in this comparison of the structures of **1** and **2** for all the lanthanides, the complexes of Ln = Eu, Yb, Sm, and Tm fall into one class and the complexes of Ln = La, Ce, Pr, Nd, Gd, Tb, Dy, Ho, Er, and Lu fall into the other class.

The data on **1** and **2** for Ln = Dy and Nd contrast with most of the data in the literature to date on Dy^{2+} and Nd^{2+} complexes. In general, Shannon radii for eight-coordinate Dy^{2+} and Nd^{2+} are 0.163 and 0.181 Å larger than those of Dy^{3+} and Nd^{3+}, respectively.[37] These numbers are based on solid state structures obtained up to 1976 before molecular examples of Dy^{2+} and Nd^{2+} were known.[9,10] Molecular examples of these ions also show the same trend. For example, the Ln–I distances in NdI$_2$(THF)$_5$[10] are 0.22 Å larger than those in [NdI$_2$(THF)$_5$]$^{1+}$.[36] A Dy^{3+} analog of DyI$_2$(DME)$_3$[9] is not available for comparison, but the Dy–I distances are actually longer than expected compared to the analogous isomorphous SmI$_2$(DME)$_3$,[82] which has long Sm–I distances typical of a 4f^{n+1} Sm^{2+} ion.

Table 2. Experimental and Calculated Average Ln−(Cp′ Centroid) Distances (Å) in Cp′$_3$Ln, 1, and [K(2.2.2-cryptand)][Cp′$_3$Ln], 2, for the Traditional Six +2 Ions, Eu, Yb, Sm, Tm, Dy, and Nd, Listed in the Order of Ln^{3+}/Ln^{2+} Reduction Potentials (Table 1)[17,22]

compd	experimental		calculated	
	Ln−(Cp′ centroid)$_{avg}$	difference	Ln−(Cp′ centroid)$_{avg}$	difference
1-Eu/2-Eu	2.451/2.607	0.156	2.485/2.604	0.117
1-Yb/2-Yb	2.365/2.508	0.143	2.391/2.495	0.104
1-Sm/2-Sm	2.461/2.608	0.147	2.470/2.600	0.130
1-Tm/2-Tm	2.379/2.502	0.123	2.385/2.501	0.116
1-Dy/2-Dy	2.407/2.443	0.036	2.490/2.563	0.073
1-Nd/2-Nd	2.489/2.519	0.030	2.489/2.509	0.020

In the course of this structural analysis, Si−C bond distances were also analyzed for **1** and **2**, since it has been suggested that the electron added to **1** to make **2** could go into the ligands and be reflected in longer Si−C(Me) or Si−C(ring) bonds.[33] Full data are given in the Supporting Information, but there is no discernible difference between the Si−C distances in **1** and **2** for any of the metals. For example, the average Si−C(Me) distance for **2-Y** is 1.872 Å vs 1.868 Å for **1-Y**. This is quite similar to the average Si−C(Me) distances of 1.873 Å for **2-Eu** and 1.867 Å for **1-Eu**.

UV−Visible Spectroscopy. The UV−vis spectra of **2-La**, **2-Ce**, **2-Dy**, and **2-Nd** are shown in Figure 3 along with the
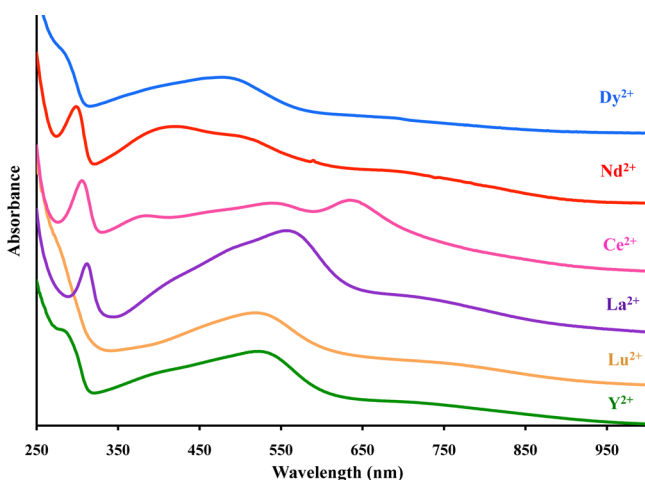

Figure 3. Stacked plot of experimental UV−vis spectra of [K(2.2.2-cryptand)][Cp′$_3$Ln], **2**, for Ln = La, Ce, Nd, and Dy in comparison to Y and Lu, in THF at 298 K. Maximum extinction coefficients for absorption at wavelengths greater than 350 nm (M^{-1} cm^{-1}) follow: Y (4500), Lu (4500), La (4400), Ce (4700), Nd (4700), Dy (3400).

spectra for **2-Y**, which necessarily contains a 4d^1 ion, and **2-Lu**, which is a 5d^1 complex since the f shell of the 4f^{14} Lu^{3+} ion is filled. These spectra are very similar to those of **2-Gd**, **2-Tb**, **2-Ho**, and **2-Er** complexes previously analyzed to have 4f^{n}5d^1 ground states.[32,33] Each complex has intense absorptions with extinction coefficients of 3000−4000 M^{-1} cm^{-1} in the high energy visible region. The spectra differ greatly from those of the corresponding Ln^{3+} complexes **1**. The +3 complexes have low extinction coefficients, since the 4f−4f transitions are Laporte forbidden, and display narrow line widths, since vibronic broadening is minimal due to the limited radial extension of the 4f orbitals.

The UV−vis spectra of **2-Eu**, **2-Yb**, **2-Sm**, and **2-Tm** are dramatically different from those of the other [K(2.2.2-

cryptand)][Cp′$_3$Ln] complexes as shown in Figure 4. For these four metals, the absorptions have lower extinction
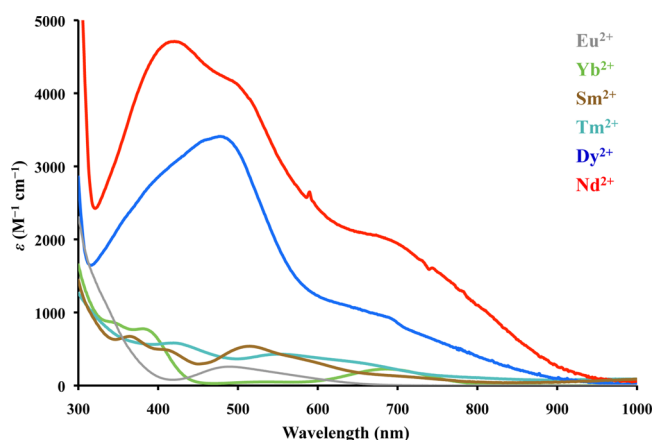
Figure 4. Experimental UV−vis spectra of [K(2.2.2-cryptand)]-[Cp′$_3$Ln], **2** (Ln = Nd, Sm, Eu, Dy, Tm, Yb), in THF at 298 K.

coefficients, $\varepsilon \leq 900$ M^{-1} cm^{-1}, compared to the other **2-Ln** complexes including **2-Dy** and **2-Nd**, also shown for comparison in Figure 4. This difference in absorbance is visually noticeable: solutions of **2-Eu**, **2-Yb**, **2-Sm**, and **2-Tm** are less intensely colored than those of the other analogs of **2**. The absorptions of the traditional 4f^{n+1} Ln^{2+} ions are attributed to Laporte allowed 4f−5d transitions.[76]

■ THEORETICAL ANALYSIS

Density functional theory (DFT) calculations were performed on both Cp′$_3$Ln, **1**, and [Cp′$_3$Ln]$^{1−}$, **2**, for the six lanthanides that traditionally have +2 oxidation states, Ln = Eu, Yb, Sm, Tm, Dy, and Nd, to compare with the calculations reported earlier on the new divalent ions.[32,33]

Ln^{3+}. Because of the presence of many low-lying excited states and small HOMO−LUMO gaps, self-consistent field calculations of open-shell lanthanide compounds are notoriously difficult to converge. Nevertheless, calculations on the Ln^{3+} complexes **1** converged smoothly in each case except for Dy. For Eu, Yb, Sm, Tm, and Nd, the lowest energy structures matched crystallographic data within a few hundredths of an angstrom (Table 2) as observed previously for the other lanthanides.[32,33] In the case of the 4f^9 Dy^{3+} ion, convergence thresholds were initially lowered and Fermi smearing of occupation numbers with simulated annealing was used.[83] Once a reasonable structure was obtained, energy and density thresholds were tightened and the calculation converged to an integer 4f^9 occupation.

Eu²⁺, Yb²⁺, Sm²⁺, and Tm²⁺. The computed structures of the anionic complexes **2**, [Cp′₃Ln]¹⁻, for the four metals, Ln = Eu, Yb, Sm, and Tm, agree well with the structural and spectroscopic data presented above. For each of these metals, the calculations predict structures of **2** that match the experimental data (Table 2). For these four metals, the differences between the Ln−(Cp′ centroid) distances of the calculated structures of **1** and **2** are significantly larger than the 0.023−0.034 Å difference calculated for Ln = Pr, Gd, Tb, Ho, Er, Y, and Lu.[32,33] Specifically, the DFT calculated Ln³⁺/Ln²⁺ bond length differences for these four metals in **2** vs **1** are Eu, 0.12 Å; Yb, 0.10 Å; Sm, 0.13 Å; Tm, 0.12 Å. The calculations agree with the larger differences found for these ions experimentally in this paper and in other studies.[9,10,18,34−37,82]

The calculations on Eu, Yb, Sm, and Tm also reveal a different character of the LUMO of the trivalent **1** and the HOMO of the anion of divalent **2** compared to the other metals. For Ln = Pr, Gd, Tb, Ho, Er, Y, and Lu, both the LUMO of **1** and HOMO of **2** appear to be almost identical d$_{z^2}$ orbitals.[32,33] However, for Eu and Yb, the LUMO of **1** and the HOMO of **2** are similar six-lobe 4f-like orbitals (Supporting Information). For Sm and Tm, the LUMO of **1** and the HOMO of **2** differ: the LUMO of **1** is a six-lobe 4f orbital, while the HOMO of **2** resembles a 4f orbital with eight lobes, Figure 5 (Supporting Information for Sm). The LUMOs of **1**
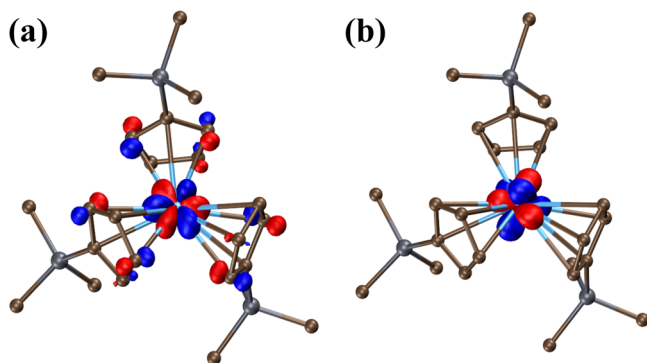
Figure 5. Molecular orbital plots of (a) the 134a orbital (LUMO) of **1-Tm** and (b) the 133a orbital (HOMO) of the anion in **2-Tm**, using a contour value of 0.05.

for these four ions have significant ligand character as shown in Figure 5 for **1-Tm** which has 41% ligand character by Mulliken population analysis.[84] The fully optimized structures of the anion of **2-Ln** for Ln = Eu, Yb, Sm, and Tm all contain an entirely metal-based HOMO.

The energy difference between 4f^{n+1} and 4f^{n}5d^1 configurations for Eu, Yb, Sm, and Tm was estimated by the Δ self-consistent field method. This resulted in 4f to 5d transfer energies of 51.8 kcal/mol (18 100 cm⁻¹) for Eu, 49.6 kcal/mol (17 300 cm⁻¹) for Yb,[85] and 29.3 kcal/mol (10 200 cm⁻¹) for Tm. These numbers can be compared with the differences between the 4f^n and 4f^{n}5d^1 levels obtained experimentally from atomic spectra of the Ln²⁺ ions: Eu, 96.9 kcal/mol (33 900 cm⁻¹); Yb, 95.5 kcal/mol (33 400 cm⁻¹); Sm, 70.0 kcal/mol (24 500 cm⁻¹); Tm, 65.5 kcal/mol (22 900 cm⁻¹).[86]

Natural population analysis (NPA) supports the notion that the Ln²⁺ complexes, [Cp′₃Eu]¹⁻, [Cp′₃Yb]¹⁻, [Cp′₃Sm]¹⁻, and [Cp′₃Tm]¹⁻, each have approximately one electron added to the f orbitals in comparison to the Ln³⁺ Cp′₃Ln complexes, Table 3. This suggests 4f^7, 4f^{14}, 4f^6, and 4f^{13} ground states for

Table 3. NPA Comparison between Cp′₃Ln and [Cp′₃Ln]¹⁻ ^{a}

| | Cp′₃Ln/[Cp′₃Ln]¹⁻ | | difference | |
Ln	4f e¹⁻	4d and 5d e¹⁻	4f e¹⁻	4d and 5d e¹⁻
Eu	6.556/6.952	10.989/10.675	+0.396	−0.214
Yb	13.465/13.919	10.989/10.725	+0.454	−0.264
Sm	5.373/5.927	11.111/10.702	+0.554	−0.409
Tm	12.277/12.911	11.110/10.746	+0.634	−0.364
Dy	8.936/8.981	11.062/10.899	+0.045	−0.163
Nd	3.221/3.530	11.188/11.177	+0.309	−0.011
La	0.016/0.018	0.934/1.222	+0.002	+0.288

^{a}The number of 4f electrons (left) and the number of 4d and 5d electrons combined (right) are compared for the two complexes.

[Cp′₃Eu]¹⁻, [Cp′₃Yb]¹⁻, [Cp′₃Sm]¹⁻, and [Cp′₃Tm]¹⁻, respectively. This matches all previous data on +2 ions of these metals including the structurally similar [K(18-crown-6)(toluene)₂][Cp″₃Sm].[35] Specifically, Table 3 shows that for Eu, Yb, Sm, and Tm, the sum of 4d and 5d electron density does not change much between the Ln³⁺ complex and the Ln²⁺ complex and even decreases, whereas the 4f electron density increases from the +3 ion to the +2 ion. For Nd and Dy, the changes in 4f and 5d population are smaller. This can be attributed to partially mixed 4f/5d ground-state configurations. The situation for La is very different: each ion has very little 4f character, and the 5d population increases.

The UV−vis spectra of **2-Ln** were simulated using TDDFT calculations that take into account solvent effects via a continuum solvent model COSMO.[65] Figure 6 shows the experimental and calculated spectra for these Ln²⁺ complexes.
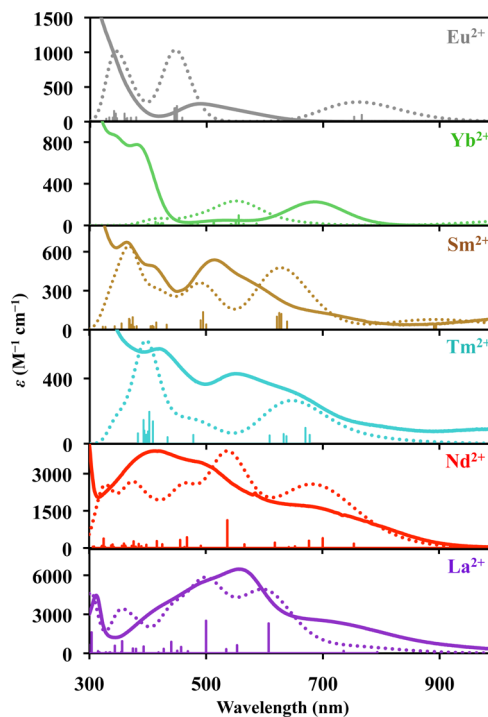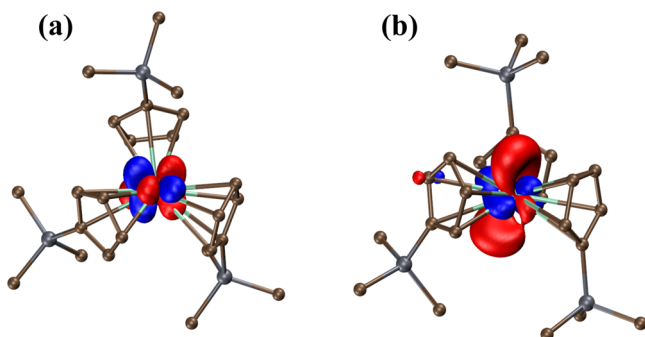

Figure 6. Experimental (solid) and calculated (dotted) UV−vis spectra of [K(2.2.2-cryptand)][Cp′₃Ln], **2** (Ln = Eu, Yb, Sm, Tm, Nd), in THF at 298 K, with pertinent theoretical excitations shown as vertical lines and theoretical extinction coefficients scaled up by a factor to best match the experimental. Calculated UV−vis spectra for **2-Dy** are shown in Figure 9.

Examination of the largest calculated transitions in the spectra of the Eu, Yb, Sm, and Tm complexes corroborates the traditional view that the absorptions arise from 4f–5d transitions[76] (see Table S19 in the Supporting Information). Several transitions originate from primarily occupied 4f orbitals that lie below the HOMO level to the 5d LUMO.

Nd²⁺. In the case of Ln = Nd, the LUMO of **1-Nd** has primarily 4f orbital character, but the HOMO of **2-Nd** has d_{z^2} orbital character, Figure 7. Although there is no requirement

Figure 8. Molecular orbital plots of (a) the 134a orbital (LUMO) of **1-Dy** and (b) the 130a orbital (HOMO) of the anion in **2-Dy**, using a contour value of 0.05.

The UV–vis spectra of **2-Dy** were also simulated for both the ground state $4f^{10}$ configuration and a higher lying $4f^9 5d^1$ configuration, Figure 9. The simulated spectrum for the
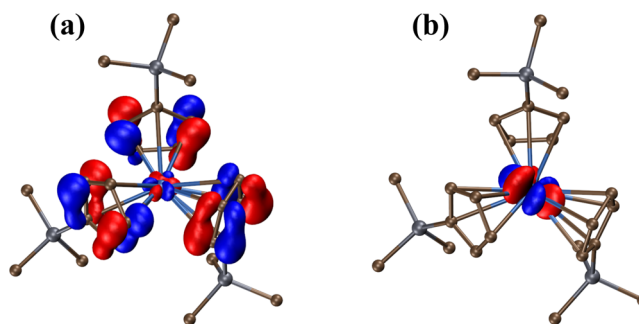

Figure 7. Molecular orbital plots of (a) the 131a orbital (LUMO) of **1-Nd** and (b) the 131a orbital (HOMO) of the anion in **2-Nd**, using a contour value of 0.05.

that the LUMO of the +3 ion should match the HOMO of the +2 ion, this Nd result differed from all previous calculations comparing **1** and **2**.[32,33] With all the other metals, the LUMO of **1** and the HOMO of **2** were either both d orbitals or both f orbitals. Close inspection of the HOMO of **2-Nd** shows that although it is primarily d_{z^2} in nature, the torus of the orbital appears to divide into four small lobes that suggest partial 4f character. Mulliken analysis[84] of this orbital suggests that the 90% metal contribution to the orbital comprises 29% d and 60% f.
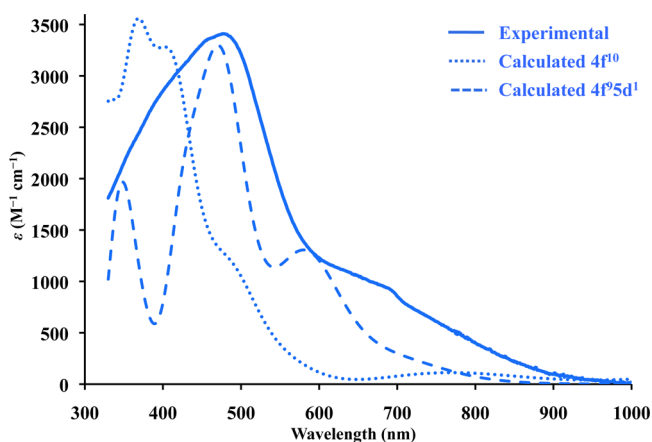
The difference in Ln−(Cp′ centroid) distances of the calculated structures of **1-Nd** and **2-Nd** was 0.020 Å, similar to the experimentally determined value, 0.030 Å. This puts Nd in the category of the Ln^{2+} complexes with $4f^n 5d^1$ configurations. The calculated Nd UV−vis spectrum is consistent with this assignment in that the major transitions are metal to ligand and not f to d as in the spectra for Eu, Yb, Sm, and Tm.

Dy²⁺. As mentioned above, the calculations for dysprosium were problematic even at the Dy³⁺ level. Calculations on **2-Dy** predicted a $4f^{10}$ configuration, i.e., a $4f^{n+1}$ configuration like that of Eu, Yb, Sm, and Tm, even though the structural and spectroscopic information suggested that Dy²⁺ is more like the Ln^{2+} complexes with $4f^n 5d^1$ configurations. The LUMO of **1-Dy** and the HOMO of **2-Dy** match: both are 4f orbitals with six lobes, Figure 8. The vertical excitation energy to the $5d^1$ occupation is calculated to be 17.8 kcal/mol. This is smaller than the 29.3−51.8 kcal/mol values calculated for Eu, Yb, and Tm (see above) and is consistent with Dy being a "crossover" element[21] in the **2** series where the 4f and 5d energy levels are so similar that there is difficulty elucidating the ground states. The difference in Ln−(Cp′ centroid) distances of the calculated structures of **1-Dy** and **2-Dy** was 0.073 Å. This is intermediate between the experimentally found 0.020−0.032 Å differences of Ln^{2+} complexes with $4f^n 5d^1$ configurations and the 0.123− 0.156 Å differences of the $4f^{n+1}$ complexes.


Figure 9. Experimental UV−vis spectrum of [K(2.2.2-cryptand)]- [Cp′₃Dy], **2-Dy**, in THF at 298 K (solid line) with calculated spectra using a $4f^{10}$ ground state configuration (dotted) and a higher lying $4f^9 5d^1$ state configuration. Theoretical extinction coefficients are scaled up by a factor of 12 000 for the $4f^{10}$ configuration and 2700 for the $4f^9 5d^1$ configuration.

$4f^9 5d^1$ case matches the experimental spectrum much better than that of the $4f^{10}$ configuration. Hence, although DFT predicts the $4f^{n+1}$ configuration to be more stable, the spectroscopic data are more consistent with a $4f^n 5d^1$ ground state.

■ DISCUSSION

Synthesis. The synthesis, isolation, and structural determination of the Cp′₃Ln, **1**, and [K(2.2.2-cryptand)][Cp′₃Ln], **2**, compounds have been accomplished for all nonradioactive lanthanides. This provides the rare opportunity to directly compare analogous complexes of all the lanthanides as well as yttrium in the same coordination environment in both the +3 and +2 oxidation states. Making direct structural and electronic comparisons of the entire rare earth series with a single ligand set is challenging, since the steric requirements for thermally stable and crystalline complexes can often change across the series as the radial size diminishes. Fortunately, this was not a problem with the $(Cp′_3)^{3-}$ ligand set with the metals in both the +2 and +3 oxidation states.

Structural Data. All members of the Cp'_3Ln, **1**, series are isomorphous; their structures vary only slightly from metal to metal because of the gradually changing radial size of the metal ion. This change in average Ln−(Cp′ centroid) distance vs atomic number, Figure 10, follows a quadratic decay as described previously in the literature.[87,88]
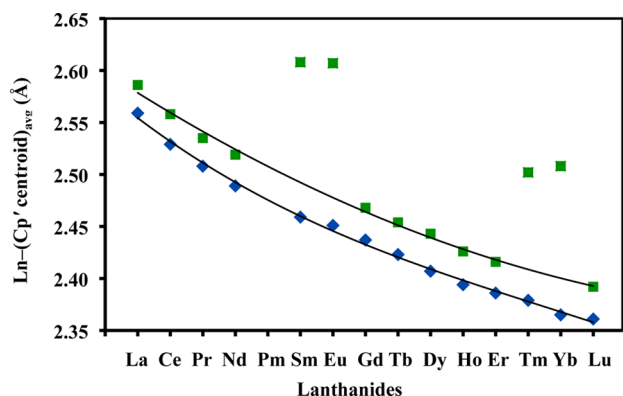
Figure 10. Plot of average Ln−(Cp′ centroid) distances in Cp'_3Ln, **1** (blue diamonds), and in $[K(2.2.2\text{-cryptand})][Cp'_3Ln]$, **2** (green squares), for each lanthanide metal.

Since the average Ln−(Cp′ centroid) distances in $[K(2.2.2\text{-cryptand})][Cp'_3Ln]$, **2**, for La, Ce, Pr, Nd, Gd, Tb, Dy, Ho, Er, and Lu are about 0.03 Å longer than those in the corresponding complexes of **1**, plotting these distances for these metals in Figure 10 gives a curve that is similar to that for the complexes of the +3 ions. Since the differences in Ln−(Cp′ centroid) bond distances for **1** vs **2** with Ln = Eu, Yb, Sm, and Tm, 0.123−0.156 Å, are much larger than the 0.03 Å difference for the other metals, their points lie significantly above the trend lines in Figure 10.

The structural differences between the complexes of Eu, Yb, Sm, Tm and the complexes of the 10 other lanthanides, La, Ce, Pr, Nd, Gd, Tb, Dy, Ho, Er, and Lu, as well as Y, can be explained by two different electron configurations for their Ln^{2+} ions. With Eu, Yb, Sm, and Tm, large differences are found because reduction of a $4f^n\ Ln^{3+}$ ion generates a $4f^{n+1}\ Ln^{2+}$ ion. Since there is little interaction of the 4f orbitals with the ligands, the bond distances are simple sums of ionic radii. Since the ionic radii of $4f^{n+1}\ Ln^{2+}$ ions are typically 0.1−0.2 Å larger than the $4f^n\ Ln^{3+}$ ions,[37] the metal−ligand bond distances in the complexes are similarly larger. With La, Ce, Pr, Nd, Gd, Tb, Dy, Ho, Er, and Lu, small differences are found because reduction of a $4f^n\ Ln^{3+}$ ion generates a $4f^n5d^1\ Ln^{2+}$ ion for the lanthanides and a $4d^1$ ion for yttrium. Since the d orbitals can interact with the ligands, the bond distances are not necessarily simple sums of ionic radii. This is typical in transition metal complexes in which many factors contribute to bond distances and simple correlations with oxidation states are not observed.[41]

Spectral Data. The UV−vis spectral data on the complexes, $[K(2.2.2\text{-cryptand})][Cp'_3Ln]$, **2**, match the structural results above. The set of four ions, Eu^{2+}, Yb^{2+}, Sm^{2+}, and Tm^{2+}, in **2** display different UV−vis spectra from those of the rest. The spectra for La^{2+}, Ce^{2+}, Pr^{2+}, Nd^{2+}, Gd^{2+}, Tb^{2+}, Dy^{2+}, Ho^{2+}, and Er^{2+} have overall shapes and intensities similar to those seen for the Y^{2+} and Lu^{2+} ions that are necessarily $4d^1$ and $4f^{14}5d^1$ systems, respectively.[31−33] The DFT calculations indicate that they arise from metal to ligand transitions. The spectra for Eu^{2+},

Yb^{2+}, Tm^{2+}, and Sm^{2+} complexes of **2** have different shapes and are weaker in intensity than the $4f^n5d^1$ complexes. They can be modeled as 4f−5d transitions occurring from a $4f^{n+1}$ ground state.[76]

"Set of Four" vs "Traditional Six" Ln^{2+} Ions. An unusual feature about the structural and spectroscopic data reported here is that complexes of Dy^{2+} and Nd^{2+} ions have properties consistent with $4f^n5d^1$ configurations rather then the traditional $4f^{n+1}$ configurations obtained by adding an electron to a $4f^n\ Ln^{3+}$ ion. The data in this study suggest that the $(Cp'_3)^{3-}$ ligand set can change the ground state from $4f^{n+1}$ to $4f^n5d^1$ for these two ions. Hence, the previous classification of +2 lanthanide ions into the traditional six $4f^{n+1}$ ions with Ln = Eu, Yb, Sm, Tm, Dy, and Nd and the nontraditional $4f^n5d^1$ ions with Ln = La, Ce, Pr, Gd, Tb, Ho, Er, and Lu and $4d^1$ Y must be modified in the sense that this dichotomy is apparently dependent on the ligand environment. In some coordination environments, specifically the $(Cp'_3)^{3-}$ ligand set, Dy and Nd can adopt the $4f^n5d^1$ electron configuration. With this $(Cp'_3)^{3-}$ set of ligands, there are only four traditional $4f^{n+1}\ Ln^{2+}$ ions.

Solid State Precedent for $4f^n5d^1$ Character in Nd^{2+} and Dy^{2+} Complexes. In 1976, a high pressure study of NdI_2 indicated that the pseudo-alkaline-earth SrI_2 structure of this compound consistent with the salt, $Nd^{2+}(I^{1-})_2$, changed with pressure to give a structure like the $Ln^{3+}(I^{1-})_2(e^{1-})$ structures found for La, Ce, and Pr.[89] This was interpreted as a crossover from a $4f^4$ to a $4f^35d^1$ configuration for the Nd^{2+} ion under pressure. This constitutes a solid state precedent for the molecular example of **2-Nd** that shows the variable nature of the electron configuration of Nd^{2+} depending on the coordination environment.

Another interesting solid state structure involving Nd was the complex $[(C_5H_2{}^tBu_3)_2Nd(\mu\text{-I})K(18\text{-crown-6})]$.[14] This Nd^{2+} complex had a solid state structure with the Nd−(ring centroid) distance only 0.05 Å larger than that in $(C_5H_2{}^tBu_3)_2Nd(\mu\text{-Cl})AlMe_3$,[90] the closest example cited for comparison. This 0.05 Å distance was the smallest increase of bond distances in a Nd^{3+} complex vs a Nd^{2+} complex observed to date for traditional Ln^{2+} complexes and seemed strange. In light of the structure of **2-Nd**, this may suggest that this is related to the variable character of Nd^{2+} electron configurations depending on coordination environment. This difference taken with the somewhat smaller than expected difference of **2-Tm** vs **1-Tm**, namely, 0.12 Å, may be indications of a continuum of bond distances in Ln^{2+} complexes that have $4f^{n+1}$ and $4f^n5d^1$ configurations of similar energy.

When this $[(C_5H_2{}^tBu_3)_2Nd(\mu\text{-I})K(18\text{-crown-6})]$ complex was published, its structural parameters were compared[14] favorably with the Dy^{2+} complexes $[(C_5H_2{}^tBu_3)_2Dy(\mu\text{-X})K(18\text{-crown-6})]$, where X = Br and BH_4.[13] We examined the metal−(ring centroid) distances for these Dy^{2+} structures compared to their Dy^{3+} analogs and found that these two pairs also show a very small difference. The difference in Ln−(ring centroid) distance for $[(C_5H_2{}^tBu_3)_2Dy(\mu\text{-Br})K(18\text{-crown-6})]$ vs $(C_5H_2{}^tBu_3)_2DyBr$ is 0.038 Å, and the difference between $[(C_5H_2{}^tBu_3)_2Dy(\mu\text{-BH}_4)K(18\text{-crown-6})]$ and $(C_5H_2{}^tBu_3)_2Dy(BH_4)$ is 0.01 Å.[13] Hence, the $[(C_5H_2{}^tBu_3)_2Dy(\mu\text{-X})K(18\text{-crown-6})]$ complexes also provide precedent for Ln^{2+} complexes whose Ln−(ring centroid) distances are not much larger than those of the Ln^{3+} analogs. It seems possible that these Dy^{2+} complexes could also have $4f^95d^1$ configurations rather than $4f^{10}$ and constitute more examples that Dy is a crossover metal in this regard.

Solid State Data on Ln^{2+} Ions in Alkaline Earth Halide Matrices. The molecular data reported here can also be compared with spectroscopic and magnetic data on solids in which Ln^{3+} ions were doped into MX_2 hosts (M = Ca, Sr, Ba; X = F, Cl) and irradiated with γ radiation from a ^{60}Co source at 77 K. The data were analyzed as arising from Ln^{2+} ions trapped in a crystalline cubic lattice of halide ions.[76,91−94] The spectroscopic data supported $4f^{n+1}$ ground states for the Ln^{2+} ions except for Gd^{2+} that "probably has f^7d for its ground configuration" and Ce^{2+} and Tb^{2+} that were considered "borderline" cases.[94] For La^{2+}, a $5d^1$ configuration was considered likely.[94,95] These results are consistent with the fact that La, Ce, Gd, and Tb have the lowest $4f^{n+1}$ to $4f^n5d^1$ promotional energies (see below). Additional spectroscopic and paramagnetic resonance data on Ho^{2+} generated under these conditions were also interpreted in terms of a $4f^{11}$ configuration.[91,92] A later study of Ce^{2+} showed data consistent with a $4f^15d^1$ ground state.[93] Subsequent analysis of the La, Ce, Gd, Tb, Lu, and Y results interpreted the data based on a model of "two electrons trapped by a trivalent-rare-earth fluorine-vacancy nearest neighbor complex."[96]

These data provide further support that the ligand field environment can affect the ground state electronic configuration of the Ln^{2+} ions. Since the ligand field splitting in a cubic environment lowers two d orbitals rather than a single d orbital as found for d_{z^2} in the trigonal environment of the $(Cp'_3)^{1-}$ ligand set, the d orbital stabilization may not be sufficient to make d orbital population energetically competitive with f orbital population. Hence, the trapped Ln^{2+} ions adopt the traditional $4f^{n+1}$ configuration in this cubic coordination environment.

DFT Calculations. The DFT calculations support the overall view that the +2 ions of Eu, Yb, Sm, and Tm in the molecular complexes **2** are different from the +2 ions of La, Ce, Pr, Gd, Tb, Ho, Er, Y, and Lu in **2** and that Dy and Nd are intermediate and could align with either group. Calculations on the complexes of the metals, Ln = La, Pr, Gd, Tb, Ho, Er, Y, and Lu, indicate the LUMOs for **1** and the HOMOs for **2** are primarily $5d_{z^2}$ ($4d_{z^2}$ for Y). In contrast, for Eu, Yb, Sm, and Tm, the LUMO for **1** and the HOMO for **2** are both 4f orbitals, with significant ligand character only observed in the LUMO for **1**. Calculations on the differences in Ln−(Cp′ centroid) distances between **1** and **2** and the UV−vis spectra for these two sets of ions fit their respective ground states.

For the two intermediate cases, Dy and Nd, the calculations indicate a near degeneracy of the $4f^{n+1}$ and $4f^n5d^1$ configurations. For such multi-reference states, the present semi-local DFT methodology cannot be expected to be accurate. In the case of Nd, the f-like LUMO of **1-Nd** does not match the d-like HOMO of **2-Nd**, but the structural difference between these compounds matches experimental data and is consistent with a $4f^35d^1$ ground state. For Dy, the ground state of the minimum energy structure for $[Cp'_3Dy]^{1-}$ does not match the best ground state for estimating the UV−vis spectra. Dy appears to be the element in the **2** series where the two electronic states are closest in energy.

A Continuum between Models. The $4f^{n+1}$ and $4f^n5d^1$ models are two extremes of a simple single electron approximation model that does not fully describe the actual electronic state in **2**. The HOMO of **2-Nd** shown in Figure 7 provides a pictorial example of this in that it has components that look both d-like and f-like. It was noted above that the differences in Ln−(Cp′ centroid) distances between **1** and **2** for

the set of four decrease in the order of their Ln^{3+}/Ln^{2+} reduction potentials: Eu, 0.156 Å, −0.35 V; Yb, 0.143 Å, −1.15 V; Sm, 0.149 Å, −1.55 V; Tm, 0.123 Å, −2.3 V.[17] The smaller difference for Tm may reflect an actual electronic state that involves a blending of both electronic extremes. The fact that Dy and Nd may be "crossover" elements that can adopt either electronic state depending on the ligand set may explain the small 0.01−0.05 Å differences between the Ln−(Cp^{ttt} centroid) distances of $[(C_5H_2{}^tBu_3)_2Nd(\mu\text{-}I)K(18\text{-crown-}6)]$[14] and $[(C_5H_2{}^tBu_3)_2Dy(\mu\text{-}X)K(18\text{-crown-}6)]$ (X = Br, BH_4)[13] and their Ln^{3+} analogs. The Nd^{2+} and Dy^{2+} ions in these complexes may have considerable $4f^n5d^1$ character.

The $4f^{n+1}$ to $4f^n5d^1$ promotion energies for free Ln^{2+} ions[86] can provide information about the relative accessibility of the 5d orbitals from metal to metal. In Figure 11, the $4f^{n+1}$ to
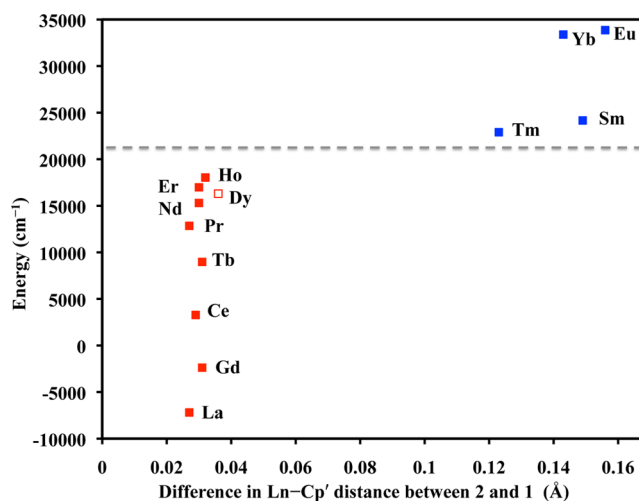
Figure 11. Plot of the $4f^{n+1}$ to $4f^n5d^1$ promotion energies (only an estimated energy is available for Dy) vs the differences in Ln−(Cp′ centroid) distances of **2** and **1**.[86] The gray dashed line indicates the barrier in promotion energies to reduce the $4f^n$ Cp'_3Ln to a $4f^{n+1}$ (blue squares on right) or $4f^n5d^1$ (red squares on left) configuration of $[Cp'_3Ln]^{1-}$.

$4f^n5d^1$ promotion energies are plotted against the differences in Ln−(Cp′ centroid) distance between **1** and **2**. This is a crude diagram, but it can be used to raise some questions regarding Ln^{2+} ions.

The gray dotted line above 20 000 cm^{-1} suggests there is a threshold energy level that allows the $4f^n5d^1$ configuration to be the ground state. This presumably relates to the amount of crystal field stabilization that is accessible from the $(Cp'_3)^{3-}$ ligand set in **2**. When a crystal field can stabilize a d orbital to this extent, formation of a $4f^n5d^1$ +2 ion should be possible. We are actively searching for other coordination geometries that will do that. The plot also suggests that if a ligand field could provide slightly more d orbital stabilization than found with the $(Cp'_3)^{3-}$ ligand set, Tm and Sm might also form $4f^n5d^1$ +2 ions.

This plot also shows the similarities in promotion energies between Ho and Er and Nd and Dy. The positions of Dy and Nd near the dotted line can explain why they are crossover elements that can form both $4f^{n+1}$ and $4f^n5d^1$ divalent ions. However, the similar energies of Ho and Er might suggest they could also form $4f^{n+1}$ +2 ions if promotion energy were the only factor involved. The fact that $4f^{n+1}$ complexes of Ho^{2+} and

Er^{2+} have not been identified in solution suggests that more factors are involved and this is too simplistic a view.

CONCLUSION

Direct comparison of the +3 and +2 ions of all the lanthanides (except Pm, which was not studied because of its radioactivity) in a single uniform coordination environment is now possible for the first time with the complexes, Cp'_3Ln, **1**, and [K(2.2.2-cryptand)][Cp'_3Ln], **2**, respectively. This allows comparison of the properties of **2** for the traditional six Ln^{2+} ions, Eu^{2+}, Yb^{2+}, Sm^{2+}, Tm^{2+}, Dy^{2+}, and Nd^{2+}, long known in solid state and solution chemistry with the properties of **2** with the new nine ions La^{2+}, Ce^{2+}, Pr^{2+}, Gd^{2+}, Tb^{2+}, Y^{2+}, Ho^{2+}, Er^{2+}, and Lu^{2+} recently discovered in molecular complexes via Schemes 1 and 2. The results indicate that the former grouping of the six traditional +2 ions with $4f^{n+1}$ ground states and the new nine +2 ions with $4f^n5d^1$ ground states should be modified. In the $(Cp'_3)^{3-}$ coordination environment of **2**, Dy^{2+} and Nd^{2+} have properties consistent with $4f^n5d^1$ ground states. In **2**, only four of the elements traditionally known to form +2 ions, namely, Eu, Yb, Sm, and Tm, have structural and spectroscopic properties consistent with $4f^{n+1}$ ground states. Hence, at this point we can identify three categories of Ln^{2+} ions: one group that forms traditional $4f^{n+1}$ ions, a second group that forms $4f^n5d^1$ ions, and a third group of metals that can cross over between configurations depending on the coordination environment. In the coordination environment of **2**, the first class has four members, Eu, Yb, Sm, and Tm, the second class has nine members, La, Ce, Pr, Gd, Tb, Ho, Y, Er, and Lu, and the third class has two, Dy and Nd. In other coordination environments, the numbers in each class may be different depending on the effect of the ligand field on d orbital availability. It is also possible that other categories are yet to be found.

DFT calculations on **1** and **2** are consistent with this analysis. The properties of the traditional set of four as well as the set of nine are well matched by the calculations. The problematic nature of the calculations on the crossover ions, Dy^{2+} and Nd^{2+}, is consistent with the presence of two electronic states that are close in energy for each ion. These metals could adopt either configuration depending on subtle differences in the coordination environment.

The 4f−5d promotion energies of the Ln^{2+} ions are also consistent with these three sets of Ln^{2+} ions. The four traditional divalent ions have the highest promotion energies and the new nine ions the lowest. Dy and Nd have promotion energies at the borderline between these two other sets. Since Tm, Er, Ho, Dy, and Nd all have promotion energies at the borderline, further studies of Ln^{2+} complexes should evaluate data with the possibility that either electron configuration could be present.

More generally, these results show that the ligand set can change the ground electronic state in Ln^{2+} complexes. This has not been observed with Ln^{3+} complexes where the limited radial extension of the 4f orbitals leads to minimal interaction with the ligand set and where the 5d orbitals are too high in energy to contribute significantly. For the +2 ions, the 5d orbitals are lower in energy. Apparently, with complexes of the Ln^{2+} ions, the proper ligand field can lower the energy of the 5d orbitals with respect to the 4f orbitals such that 5d can be part of the ground state. The trigonal environment of the $(Cp'_3)^{3-}$ ligand set is ideal for this purpose, since a single d orbital is stabilized.

In these special ligand fields, the $4f^n5d^1$ configuration is more accessible than the $4f^{n+1}$ ground state for most of the lanthanides so that reduction of Ln^{3+} to Ln^{2+} is possible with potassium. The Ln^{3+}/Ln^{2+} redox potentials calculated for $4f^n$ Ln^{3+} to $4f^{n+1}$ Ln^{2+} reduction, Table 1, do not apply in the ligand environments that stabilize the 5d orbitals. It will be interesting to determine the range of ligand environments that will stabilize the 5d orbitals and if the accessibility of the 5d orbitals will allow isolation of complexes of Ln^{1+}.

ASSOCIATED CONTENT

Ⓢ Supporting Information

Additional computational details, spectroscopic information, crystallographic data collection, structure solution, and refinement (PDF); X-ray diffraction details of compounds **2-La** (CCDC no. 1025259), **2-Ce** (1025260), **2-Nd** (1025261), **1-Sm** (1025315), **2-Sm** (1025262), **1-Eu** (1025316), **2-Eu** (1025374), **1-Dy** (1025317), **2-Dy** (1025375), **1-Tm** (1025318), **2-Tm** (1025376), **1-Yb** (1025319), and **2-Yb** (1025377) (CIF); and DFT-optimized structural coordinates for **1-Nd**, **1-Sm**, **1-Eu**, **1-Dy**, **1-Tm**, **1-Yb**, and the anions in **2-Nd**, **2-Sm**, **2-Eu**, **2-Dy**, **2-Tm**, and **2-Yb** (XYZ). This material is available free of charge via the Internet at http://pubs.acs.org.

AUTHOR INFORMATION

Corresponding Authors
filipp.furche@uci.edu
wevans@uci.edu

Notes
The authors declare no competing financial interest.

ACKNOWLEDGMENTS

REFERENCES

(1) Meyer, G. In *The Rare Earth Elements: Fundamentals and Applications*; Atwood, D. A., Ed.; Wiley: Chichester, U.K., 2012.

(2) Matignon, C.; Cazes, E. C. *Ann. Chim. Phys.* **1906**, *8*, 417−426.

(3) Jantsch, G.; Skalla, N. *Z. Anorg. Allg. Chem.* **1929**, *185*, 49−64.

(4) Klemm, W.; Bommer, H. *Z. Anorg. Allg. Chem.* **1937**, *231*, 138−171.

(5) Corbett, J. D. *Rev. Chim. Miner.* **1972**, *10*, 289.

(6) Meyer, G. *Chem. Rev.* **1988**, *88*, 93−107.

(7) Meyer, G. *Z. Anorg. Allg. Chem.* **2007**, *633*, 2537−2552.

(8) Bochkarev, M. N.; Fedushkin, I. L.; Fagin, A. A.; Petrovskaya, T. V.; Ziller, J. W.; Broomhall-Dillard, R. N. R.; Evans, W. J. *Angew. Chem., Int. Ed. Engl.* **1997**, *36*, 133−135.

(9) Evans, W. J.; Allen, N. T.; Ziller, J. W. *J. Am. Chem. Soc.* **2000**, *122*, 11749−11750.

(10) Bochkarev, M. N.; Fedushkin, I. L.; Dechert, S.; Fagin, A. A.; Schumann, H. *Angew. Chem., Int. Ed.* **2001**, *40*, 3176−3178.

(11) Evans, W. J. *Coord. Chem. Rev.* **2000**, *206*, 263−283.

(12) Evans, W. J. *Inorg. Chem.* **2007**, *46*, 3435−3449.

(13) Jaroschik, F.; Nief, F.; Le Goff, X.-F.; Ricard, L. *Organometallics* **2007**, *26*, 1123−1125.

(14) Jaroschik, F.; Momin, A.; Nief, F.; Le Goff, X.-F.; Deacon, G. B.; Junk, P. C. *Angew. Chem., Int. Ed.* **2009**, *48*, 1117−1121.

(15) Meyer, G.; Meyer, H.-J. *Chem. Mater.* **1992**, *4*, 1157−1168.

(16) Meyer, G.; Wickleder, M. S. *Handbook on the Physics and Chemistry of Rare Earths*; Elsevier Science B. V.: Amsterdam, 2000; Vol. 28.

(17) Morss, L. R. *Chem. Rev.* **1976**, *76*, 827−841.

(18) Bochkarev, M. N. *Coord. Chem. Rev.* **2004**, *248*, 835−851 and references therein.

(19) Nief, F. *Dalton Trans.* **2010**, *39*, 6589−6598 and references therein.

(20) Corbett, J. D. *Rev. Chim. Miner.* **1973**, *10*, 239−257.

(21) Meyer, G. *Angew. Chem., Int. Ed.* **2008**, *47*, 4962−4964.

(22) Mikheev, N. B.; Auerman, L. N.; Rumer, I. A.; Kamenskaya, A. N.; Kazakevich, M. Z. *Russ. Chem. Rev.* **1992**, *61*, 1805.

(23) Connelly, N. G.; Geiger, W. E. *Chem. Rev.* **1996**, *96*, 877−910.

(24) Gun'ko, Y. K.; Hitchcock, P. B.; Lappert, M. F. *J. Organomet. Chem.* **1995**, *499*, 213−219.

(25) Al-Juaid, S.; Gun'ko, Y. K.; Hitchcock, P. B.; Lappert, M. F.; Tian, S. J. *J. Organomet. Chem.* **1999**, *582*, 143−152.

(26) Bochkarev, M. N.; Fagin, A. A. *Chem.—Eur. J.* **1999**, *5*, 2990−2992.

(27) Hitchcock, P. B.; Lappert, M. F.; Tian, S. *Organometallics* **2000**, *19*, 3420−3428.

(28) Evans, W. J.; Allen, N. T.; Ziller, J. W. *Angew. Chem., Int. Ed.* **2002**, *41*, 359−361.

(29) Nief, F.; Turcitu, D.; Ricard, L. *Chem. Commun.* **2002**, 1646−1647.

(30) Hitchcock, P. B.; Lappert, M. F.; Maron, L.; Protchenko, A. V. *Angew. Chem., Int. Ed.* **2008**, *47*, 1488−1491.

(31) MacDonald, M. R.; Ziller, J. W.; Evans, W. J. *J. Am. Chem. Soc.* **2011**, *133*, 15914−15917.

(32) MacDonald, M. R.; Bates, J. E.; Fieser, M. E.; Ziller, J. W.; Furche, F.; Evans, W. J. *J. Am. Chem. Soc.* **2012**, *134*, 8420−8423.

(33) MacDonald, M. R.; Bates, J. E.; Ziller, J. W.; Furche, F.; Evans, W. J. *J. Am. Chem. Soc.* **2013**, *135*, 9857−9868.

(34) Evans, W. J.; Foster, S. E. *J. Organomet. Chem.* **1992**, *433*, 79−94.

(35) Gun'ko, Y. K.; Hitchcock, P. B.; Lappert, M. F. *Chem. Commun.* **1998**, 1843−1844.

(36) Huebner, L.; Kornienko, A.; Emge, T. J.; Brennan, J. G. *Inorg. Chem.* **2004**, *43*, 5659−5664.

(37) Shannon, R. D. *Acta Crystallogr., Sect. A* **1976**, *32*, 751−767.

(38) Evans, W. J.; Grate, J. W.; Choi, H. W.; Bloom, I.; Hunter, W. E.; Atwood, J. L. *J. Am. Chem. Soc.* **1985**, *107*, 941−946.

(39) Evans, W. J.; Ulibarri, T. A.; Chamberlain, L. R.; Ziller, J. W.; Alvarez, D. J. *Organometallics* **1990**, *9*, 2124−2130.

(40) Evans, W. J.; Keyer, R. A.; Ziller, J. W. *J. Organomet. Chem.* **1990**, *394*, 87−97.

(41) For example, Cp_2TiCl_2 (Clearfield, A.; Warner, D. K.; Saldarriaga-Molina, C. H.; Ropal, R.; Bernal, I. *Can. J. Chem.* **1975**, *53*, 1622−1629) and $[Cp_2Ti(\mu\text{-}Cl)]_2$ (Jungst, R.; Sekutowski, D.; Davis, J.; Luly, M.; Stucky, G. *Inorg. Chem.* **1977**, *16*, 1645−1655) have average $C(\eta^5\text{-}Cp)$ bond lengths of 2.370 and 2.350 Å, respectively. Similarly, Cp_4Zr (Rogers, R. D.; Bynum, R. V.; Atwood, J. L. *J. Am. Chem. Soc.* **1978**, *100*, 5238−5239) and Cp_3Zr (Lukens, W. L., Jr.; Andersen, R. A. *Organometallics* **1995**, *14*, 3435−3439) both have the same average $Zr\text{-}C(\eta^5\text{-}Cp)$ bond length of 2.58 Å.

(42) Lauher, J. W.; Hoffmann, R. *J. Am. Chem. Soc.* **1976**, *98*, 1729−1742.

(43) Bursten, B. E.; Rhodes, L. F.; Strittmatter, R. J. *J. Am. Chem. Soc.* **1989**, *111*, 2758−2766.

(44) Bursten, B. E.; Rhodes, L. F.; Strittmatter, R. J. *J. Am. Chem. Soc.* **1989**, *111*, 2756−2758.

(45) Strittmatter, R. J.; Bursten, B. E. *J. Am. Chem. Soc.* **1991**, *113*, 552−559.

(46) Denning, R. G.; Harmer, J.; Green, J. C.; Irwin, M. *J. Am. Chem. Soc.* **2011**, *133*, 20644−20660.

(47) Lukens, W. W., Jr.; Andersen, R. A. *Organometallics* **1995**, *14*, 3435−3439.

(48) Taylor, M. D. *Chem. Rev.* **1962**, *62*, 503−511.

(49) Girard, P.; Namy, J. L.; Kagan, H. B. *J. Am. Chem. Soc.* **1980**, *102*, 2693−2698.

(50) Heckmann, G.; Niemeyer, M. *J. Am. Chem. Soc.* **2000**, *122*, 4227−4228.

(51) Izod, K.; Liddle, S. T.; Clegg, W. *Inorg. Chem.* **2004**, *43*, 214−218.

(52) Bergbreiter, D. E.; Killough, J. M. *J. Am. Chem. Soc.* **1978**, *100*, 2126−2134.

(53) Jordan, R. F.; Echols, S. F. *Inorg. Chem.* **1987**, *26*, 383−386.

(54) Peterson, J. K.; MacDonald, M. R.; Ziller, J. W.; Evans, W. J. *Organometallics* **2013**, *32*, 2625−2631.

(55) Stults, S. D.; Andersen, R. A.; Zalkin, A. *Organometallics* **1990**, *9*, 115−122.

(56) Krinsky, J. L.; Minasian, S. G.; Arnold, J. *Inorg. Chem.* **2011**, *50*, 345−357.

(57) Minasian, S. G.; Krinsky, J. L.; Rinehart, J. D.; Copping, R.; Tyliszczak, T.; Janousch, M.; Shuh, D. K.; Arnold, J. *J. Am. Chem. Soc.* **2009**, *131*, 13767−13783.

(58) Lappert, M. F.; Yarrow, P. I. W.; Atwood, J. L.; Shakir, R.; Holton, J. *J. Chem. Soc., Chem. Commun.* **1980**, 987−988.

(59) Staroverov, V. N.; Scuseria, G. E.; Tao, J.; Perdew, J. P. *J. Chem. Phys.* **2003**, *119*, 12129−12137.

(60) Bates, J. E.; Furche, F. *J. Chem. Phys.* **2012**, *137*, 164105/1−16105/10.

(61) *TURBOMOLE*, version 6.5; TURBOMOLE GmbH: Karlsruhe, Germany, 2013; http://www.turbomole.com.

(62) Cao, X.; Dolg, M. *J. Mol. Struct.: THEOCHEM* **2002**, *581*, 139−147.

(63) Weigend, F.; Ahlrichs, R. *Phys. Chem. Chem. Phys.* **2005**, *7*, 3297−3305.

(64) Rappoport, D.; Furche, F. *J. Chem. Phys.* **2010**, *133*, 134105/1−134105/11.

(65) Klamt, A.; Schueuermann, G. *J. Chem. Soc., Perkin Trans. 2* **1993**, 799−805.

(66) *CRC Handbook of Chemistry and Physics*, 81st ed.; Lide, D. R., Ed.; CRC Press: Boca Raton, FL, 2008; Chapter 8, p 136.

(67) Bauernschmitt, R.; Ahlrichs, R. *Chem. Phys. Lett.* **1996**, *256*, 454−464.

(68) Tilley, T. D.; Anderson, R. A.; Spencer, B.; Ruben, H.; Zalkin, A.; Templeton, D. H. *Inorg. Chem.* **1980**, *19*, 2999−3003.

(69) Spirlet, M.-R.; Goffart, J. *J. Organomet. Chem.* **1995**, *493*, 149−151.

(70) Cassani, M. C.; Lappert, M. F.; Laschi, F. *Chem. Commun.* **1997**, 1563−1564.

(71) Kot, W. K.; Shalimoff, G. V.; Edelstein, N. M.; Edelman, M. A.; Lappert, M. F. *J. Am. Chem. Soc.* **1988**, *110*, 986−987.

(72) Blake, P. C.; Edelstein, N. M.; Hitchcock, P. B.; Kot, W. K.; Lappert, M. F.; Shalimoff, G. V.; Tian, S. *J. Organomet. Chem.* **2001**, *636*, 124−129.

(73) Walensky, J. R.; Martin, R. L.; Ziller, J. W.; Evans, W. J. *Inorg. Chem.* **2010**, *49*, 10007−10012.

(74) Parry, J. S.; Geoffrey, G. L.; Coles, S. J.; Hursthouse, M. B. *J. Am. Chem. Soc.* **1999**, *121*, 6867−6871.

(75) Siladke, N. A.; Webster, C. L.; Walensky, J. R.; Takase, M. K.; Ziller, J. W.; Grant, D. J.; Gagliardi, L.; Evans, W. J. *Organometallics* **2013**, *32*, 6522−6531.

(76) Dieke, G. H.; Crosswhite, H. M.; Crosswhite, H. *Spectra and Energy Levels of Rare Earth Ions in Crystals*; Interscience Publishers: New York, 1968.

(77) Eméleus, H. J.; Sharpe, A. G. *Modern Aspects of Inorganic Chemistry*; Routledge & Kegan Paul: London, 1973; Vol. 4.

(78) Bünzli, J. C. G.; Choppin, G. R. *Lanthanide Probes in Life, Chemical, And Earth Sciences: Theory and Practice*; Elsevier: Amsterdam, 1989.

(79) Cotton, S. *Lanthanide and Actinide Chemistry*; Wiley: Chichester, U.K., 2006.

(80) Atwood, D. A. *The Rare Earth Elements: Fundamentals and Applications*; Wiley: Chichester, U.K., 2012.

(81) Evans, W. J.; Hozbor, M. A. *J. Organomet. Chem.* **1987**, *326*, 299−306.

(82) Evans, W. J.; Broomhall-Dillard, R. N. R.; Ziller, J. W. *Polyhedron* **1998**, *17*, 3361−3370.

(83) Nava, P.; Sierka, M.; Ahlrichs, R. *Phys. Chem. Chem. Phys.* **2003**, *5*, 3372−3381.

(84) Mulliken, R. S. *J. Chem. Phys.* **1955**, *23*, 1833−1840.

(85) For unknown reasons, the calculation on Sm was more difficult and a corresponding value for Sm was not obtained. The calculation for Yb used def2-SVP, while the calculations for Eu and Tm used def2-SVPD basis sets.

(86) Dorenbos, P. *J. Phys.: Condens. Matter* **2003**, *15*, 575−594.

(87) Seitz, M.; Oliver, A. G.; Raymond, K. N. *J. Am. Chem. Soc.* **2007**, *129*, 11153−11160 and references therein.

(88) Quadrelli, E. A. *Inorg. Chem.* **2002**, *41*, 167−169.

(89) Beck, H. P. *Z. Naturforsch.* **1976**, *31b*, 1548−1549.

(90) Walter, M. D.; Bentz, D.; Weber, F.; Schmitt, O.; Wolmershäuser, G.; Sitzmann, H. *New J. Chem.* **2007**, *31*, 305−318.

(91) Sabisky, E. S. *Phys. Rev.* **1966**, *141*, 352−362.

(92) Weakliem, H. A.; Kiss, Z. J. *Phys. Rev.* **1967**, *157*, 277−290.

(93) Alig, R. C.; Kiss, Z. J.; Brown, J. P.; McClure, D. S. *Phys. Rev.* **1969**, *186*, 276−284.

(94) McClure, D. S.; Kiss, Z. J. *J. Chem. Phys.* **1963**, *39*, 3251−3257.

(95) O'Connor, J. R.; Chen, J. H. *Bull. Am. Phys. Soc.* **1963**, *8*, 231.

(96) Staebler, D. L.; Schnatterly, S. E. *Phys. Rev. B* **1971**, *3*, 516−526.